The onset of purely elastic and thermo-elastic instabilities in Taylor-Couette flow: Influence of gap ratio and fluid thermal sensitivity

A Thesis Presented for
Master of Science
Degree
The University of Tennessee, Knoxville

MohammadReza Ghanbari
December 2013

ACKNOWLEDGEMENTS

Foremost, I would like to express my sincere gratitude to my advisor Prof. Bamin Khomami for the continuous support of my M.Sc. study and research, for his patience, motivation, enthusiasm, and immense knowledge. His guidance helped me in all the time of research and writing of this thesis. I could not have imagined having a better advisor and mentor for my M.Sc. study.

Besides my advisor, I would like to thank the rest of my thesis committee: Prof. Brian Edwards, and Dr. Dibyendu Mukherjee, for their encouragement, insightful comments, and hard questions.

My sincere thanks also goes to Dr. Dennis Thomas and Dr. Liu Nan-Sheng, for their great help and advice throughout my MSc thesis.

Last but not the least, I would like to thank my parents for giving birth to me at the first place and supporting me spiritually throughout my life.

ABSTRACT

Linear stability analysis of Taylor-Couette flow of dilute polymeric solutions has been performed by using two prototypical constitutive equations for polymeric solutions namely, the Oldroyd-B and the FENE-P models. The hydrodynamic stability characteristics of the flow in presence and absence of thermal effects and in the limit of vanishing fluid inertia have been determined using an eigenvalue analysis. Particular attention has been paid to accurate determination of the instability onset conditions as a function of fluid thermal sensitivity and gap ratio. We observe a reduction in the critical Deborah, De_c for the instability onset as the gap ratio and fluid thermal sensitivity is enhanced. In particular, under non-isothermal conditions, De_c is reduced by almost an order of magnitude for all gap ratios. Our results suggest that recent experiments leading to observations of "purely elastic turbulence" in the Taylor-Couette flow at order (1) De by Steinberg and Groisman (reference 17) were not performed under isothermal conditions. Hence, this new flow state should be labeled as "thermo-elastic turbulence".

TABLE OF CONTENTS

CHAPTER 1 INTRODUCTION 1
1.1. Elastic instabilities in simple curvilinear flows 1
1.2. Taylor-Couette flow system 1
1.3. Macromolecules 2
1.4. Shear-rate dependent viscosity 3
1.5. Normal stresses 4
1.6. Elastic and thermo-elastic instabilities 4
1.7. Modeling of polymeric flows 6
1.7.1. Kinetic theory of dilute polymeric solutions 7
1.7.2. Continuum level models 8
1.7.2.1. Oldroyd-B model 8
1.7.2.2. FENE-P model 11
Chapter 2 LITERATURE RIVIEW 14
2.1. Brief history of Taylor-Couette viscoelastic instabilities 14
2.2. Discrepancies in experimental and numerical studies 15
2.3. Goal of our study 19
Chapter 3 PROBLEM FORMULATION 21
3.1. Governing equations 21
3.2. Linear stability analysis and numerical implementation 27
Chapter 4 RESULTS AND DISCUSSION 29
4.1. Choice of parameters and steady-state solution 29
4.2. Linear stability analysis: purely elastic instability versus thermo-elastic instability 37
4.3. Influence of energetics 40
4.4. Influence of gap ratio and solvent viscosity 42
4.5. Influence of finite extensibility 46
Chapter 5 CONCLUSIONS 52
List of REFERENCES 53
VITA 57

LIST OF TABLES

Table 1 Critical parameters calculated via linear stability analysis (Bi=10, Br=0.0244, Pe=20000, β=0.765, ε=0.5, E=∞) 39

Table 2 Critical Deborah number calculated via linear stability analysis at various gap ratios for different maximum extensibilities (Bi=10, Br=0.0244, Pe=20000, β=0.765, ε=0.5, E=∞) 45

Table 3 Critical Deborah number calculated via linear stability analysis at different maximum extensibilities (Bi=10, Br=0.0244, Pe=20000, β=0.765, ε=0.5, E=∞) 48

LIST OF FIGURES

Figure 1 Schematic of the Taylor-Couette flow geometry 21

Figure 2 Comparison of base state solution for Oldroyd-B and FENE-P models at De=13, Bi=10, Br=0.0244, Pe=20000, β=0.765, ε=0.5 (a) V_θ and T^*T_0-273.15℃ and (b) $\tau_{r\theta}$ (shear stress) and N_1 (first normal stress) 32

Figure 3 Steady state profiles for Bi=10, Br=0.0244, Pe=20000, β=0.765, L=1000, ε=0.5 at De=0.5 and De=13 (a) and T^*T_0-273.15℃ (b) V_θ and dV_θ/dr (c) N_1 and $\tau_{r\theta}$ 33

Figure 4 Steady state profiles calculated for Bi=10, Br=0.0244, Pe=20000, β=0.765, ε=0.5 at De=0.5 (a) T^*T_0-273.15℃ (b) V_θ and dV_θ/dr (c) $\tau_{r\theta}$ (d) N_1 34

Figure 5 Steady state profiles calculated for Bi=10, Br=0.0244, Pe=20000, β=0.765, ε=0.5 at De=13 (a) T^*T_0-273.15℃ (b) V_θ and dV_θ/dr (c) $\tau_{r\theta}$ (d) N_1 35

Figure 6 Normalized trace(C) across gap for Bi=10, Br=0.0244, Pe=20000, β=0.765, ε=0.5 at a) De=0.5 b) De=13 36

Figure 7 Neutral stability curves for Bi=10, Br=0.0244, Pe=20000, β=0.765, ε=0.5 and E=∞ 38

Figure 8 Neutral stability curve for β=0.765 and ε=0.5 using FENE-P model (L=1000) 38

Figure 9 Critical Deborah (De_c) vs activation energy for Bi=10, Br=0.0244, Pe=20000, β=0.765, E=∞ using FENE-P model (L=1000) (a) ε=0.5 and (b) ε=0.1 41

Figure 10 Critical Deborah (De_c) vs gap ratio for Bi=10, Br=0.0244, Pe=20000, β=0.765 (a) isothermal and non-axisymmetric/time-dependent mode of (ξ=1) and (b) non-isothermal and symmetric/stationary mode of (ξ=0) 43

Figure 11 Critical Deborah (De_c) vs gap ratio for Bi=10, Br=0.0244, Pe=20000, β=0.765 at L=1000 and L=50 (a) isothermal and non-axisymmetric/time-dependent mode of (ξ=1) and (b) non-isothermal and symmetric/stationary mode of (ξ=0) 44

Figure 12 Critical Deborah (De_c) vs solvent to solution viscosity for L=1000, Bi=10, Br=0.0244, Pe=20000, ε=0.5 and symmetric/stationary mode of (ξ=0) 46

Figure 13 Critical Deborah (De_c) vs maximum extensibility (L) for Bi=10, Br=0.0244, Pe=20000, β=0.765 (a) Stationary and symmetric mode (ξ=0) and (b) oscillatory and non-axisymmetric mode (ξ=1) 47

Figure 14 Reduced shear viscosity versus reduced shear rate (defined as *De*) for a dilute solution of FENP dumbbells in a simple shear flow..... 49

Figure 15 Reduced first normal stress coefficient versus reduced shear rate (defined as *De*) for a dilute solution of FENP dumbbells in a simple shear flow..... 50

CHAPTER 1
INTRODUCTION

1.1. ELASTIC INSTABILITIES IN SIMPLE CURVILINEAR FLOWS

Investigating the influence of elasticity on the hydrodynamic stability of prototypical flows has been a topic of much research in the past few decades. In particular, shear flows such as Taylor-Couette, Dean, cone-and-plate and plate-plate flows have received a great deal of attention as they are prone to purely elastic instabilities. In absence of fluid inertia, purely elastic instabilities manifest as Deborah number, De which is defined as the ratio of fluid relaxation time to characteristic flow time scale, becomes $O(1)$. Although spatio-temporal characteristics of instability and non-linear flow pattern transitions are dependent on the flow geometry, purely elastic instabilities are attributed to significant polymer normal stress along the curved streamlines leading to hoop stresses. In turn, hoop stresses squeeze fluid elements radially inward and elastic instability can be triggered.

The aforementioned purely elastic as well as elastically induced hydrodynamic instabilities play a critical role not only in characterization of polymeric fluids but also in rational design and optimization liquid state processing of polymers.

1.2. TAYLOR-COUETTE FLOW SYSTEM

Motion of a fluid confined between two infinitely long and concentric rotating cylinders, is named Taylor-Couette flow due to pioneering studies by Taylor[1] demonstrating a transition from a purely azimuthal flow to a secondary flow state composed of toroidal cells stacked up along the axes of the cylinder above a critical

Reynolds number, defined as the ratio of inertial to viscous forces. Golubitsky[2], Chandrasekhar[3] and, Chossat and Iooss[4] observed similar instabilities in the Taylor-Couette system. Later, Giesekus[5] reported viscoelastic instability within the Taylor-Couette flow system. More recently, extensive research has been performed to probe the existence of purely elastic and inertio-elastic instabilities in the viscoelastic Taylor-Couette flows.[6,7,8,9,10,11,12,13 ,14]

1.3. MACROMOLECULES

Polymers are large macromolecules composed of repeating structural units. The conformation of repeating units determines the polymers 'microstructure.[15] When considering polymer molecules in a flow field and depending on the type of flow (shear, extensional or a combinatory), these molecules are prone to stretch and orient, leading to even more complex conformational modes. The contribution of conformational changes realized under flow deformations results in the viscoelastic nature of polymeric flows. Unlike Newtonian fluids, the polymeric fluids' stress tensor will depend on the history of the flow deformation, causing a spectrum of relaxation times attributed to the flow-induced or thermally-induced conformational changes. A polymer molecule's tendency under flow deformation to collapse back to its initial configuration is the deterministic criterion for elastic, viscous or viscoelastic behavior. If the flow's deformation rate is higher than relaxation rate (rate of flow-induced or thermal-induced configurational changes), the polymeric fluid will behave like an elastic solid while at low flow-deformation rates it behaves like a Newtonian fluid; hence, polymers manifest viscoelastic behavior.

Polymeric fluids can be classified in three broad categories: dilute solution, concentrated solution and melts. Dilute polymer solutions, which are examined in this study, consist of a small number of dissolved high-molecular weight polymers in a solvent. In dilute polymer solutions, polymer molecules can be considered independently; in contrast, due to entanglements and inter-molecularly dependent dynamics, the concentrated solutions and melts rheological behavior is more complicated than that of polymeric solutions.

1.4. SHEAR-RATE DEPENDENT VISCOSITY

Depending on fluid type, viscosity versus shear rate can change differently. In certain types of fluids, viscosity decreases when the shear rate increase while in other types the reverse is observed. The former type is called pseudo-plastic (shear-thinning) fluids; and the latter type is called dilatant or shear-thickening fluids. Most polymeric fluids behave as shear-thinning fluids; disentanglement of the polymer chains leads to their alignment along streamlines, and decreased friction between shear layers. Examples of shear thinning fluids include polyethylene, polypropylene, polyethylene in water and glycerin, and polyacrylamide in NaCl and water. On the other hand, titanium oxide suspended in a sucrose solution or corn-starch in an ethylene-glycol-water mixture is a shear-thickening fluid whose behavior is associated with the formation of flow-induced structures.

1.5. NORMAL STRESSES

In contrast to Newtonian fluids, polymeric fluids experience another type of stress along the flow streamlines. This type is referred to as normal stress. This stress is formed due to chain strengthening and orientation in the direction of the flow streamlines. If "1" and "2" refer to the direction of shearing flow and velocity gradient, respectively, the normal stresses are defined as the first normal stress, $N_1 = \tau_{11} - \tau_{22}$ and the second normal stress, $N_2 = \tau_{22} - \tau_{33}$ with τ referring to stress. Except for liquid crystalline polymers, N_1 is larger than N_2. N_1 is proportional to the square of shear rate; this proportionality is defined as the first normal stress coefficient. Normal stresses play the most important role in developing elastic instabilities.

1.6. ELASTIC AND THERMO-ELASTIC INSTABILITIES

Flow instabilities occur in both Newtonian and Non-Newtonian fluids. Instabilities emerge as secondary flows with different spatio-temporal features making them distinguishable from the primary base flow. The mutual interaction amid viscous, inertial and elastic forces leads to distinct flow transitions with different instability characteristics in viscoelastic curvilinear flow systems.

Several parameters can cause instabilities; chief among those parameters are the type of fluid (either Newtonian or non-Newtonian), flow geometry, and thermal characteristics of the flow system under consideration. While a Newtonian flow's inertial instabilities are characterized by Reynolds Number, Re, defined as the ratio of viscous diffusion time scale to flow time scale, purely elastic instabilities attributed to viscoelastic flows are characterized by Deborah number, De, defined as the ratio of

polymer relaxation time to flow time scale. Weissenberg number, Wi, is another parameter used to characterize the strength of elastic effects. Wi is a measure of the ratio of elastic to viscous forces.[16]

Normal stresses play a significant role in forming elastic instabilities. Polymer molecules are stretched around curved streamlines in viscoelastic curvilinear flows. Hence, elastic forces develop in the direction of the flow called, "hoop stresses". In turn, the primary shear flow becomes unstable, resulting in secondary flow.[17]

It is well known that presence of significant hoop stresses can drive purely elastic instabilities in curvilinear flows. Moreover, for thermally sensitive fluids, the critical conditions for the onset of instability can be greatly altered. Recently, a new mode of instability labeled, "thermo-elastic instability" has been discovered.[18,19,20] Specifically, in highly viscous and thermally sensitive fluids such as Boger fluids, commonly used in experimental studies of purely elastic instabilities, viscous dissipation leads to elasticity and viscosity gradients. Such gradients can be convected within the flow due to radial velocity perturbation (because of the rise of the secondary flow), resulting in thermo-elastic instability. The thermal sensitivity of a fluid is appropriately defined by the, Nahme-Griffith number, Na, the production of the Brinkman number, Br, representing the ratio of heat generation due to viscous heating to heat conduction rate, and the activation energy attributed to viscosity and relaxation time (expressed as an Arrhenius relationship[21]).[18,19,20,22]

1.7. MODELING OF POLYMERIC FLOWS

Regardless of simple or complex geometries, Newtonian and Polymeric flows' macroscopic rheological behaviors are expressed in mathematical language using the continuity equation (conservation of mass), motion equations (conservation of momentum) and constitutive equations (relating kinematics to stress). Polymeric fluids are distinguished from Newtonian fluids by their Non-Newtonian behavior; their stress tensor is non-linearly dependent on the flow's deformation-rate tensor. This dependency complicates prediction of the polymeric fluids' rheological behavior. A polymer molecule's conformation, as a dominant microstructural characteristic, is a deterministic factor in calculating the macroscopic viscoelastic stress field. This non-linearity in the flow-microstructure relationship control complicates phenomena namely: shear-thinning, stress relaxation, elastic instabilities in the absence of inertial effects, and normal stresses. Developing a model that captures polymeric fluids' rheological characteristics in simple shear and extensional flows is challenging for theoretical and computational rheologists, and such complexity arises from a huge number of microstructural degrees of freedom leading to a broad spectrum of time and length scales. Developing a model encompassing the detailed fluid physics of polymer molecules is infeasible. There are three types of modeling approaches based on the scale of interest: atomistic modeling, kinetic theory models, and continuum level. Although a complete description of all three types is beyond this study's scope, the development of continuum-based polymer models is briefly described. First, however, to understand continuum-based models, an introduction to kinetic theory is essential.

1.7.1. KINETIC THEORY OF DILUTE POLYMERIC SOLUTIONS

The behavior of polymer molecules on a mescoscopic level can be described by kinetic theory. A detailed model within the kinetic theory group is the freely-jointed, bead-rod Kramers chain model. Each bead represents one portion of the polymer chain (10-20 monomers), and all the beads are connected by massless rods. Each rod is scaled to one Kuhn length. This is the length over which monomer groups can act independently across the polymer backbone. If such a polymer chain resides in a solvent, the beads experience polymer-solvent interactions, namely hydrodynamic drag and Brownian forces. It is noteworthy that the bead-rod model does not incorporate the polymer molecule's chemical structure; however, it does contain the essential physics of stretching, orienting and deformation. In coarse-grained bead-spring model, the rods are replaced with phantom entropic springs. As the chain moves through the solvent, the beads experience drag forces, a phenomenon usually described by Stokes' law.

Further coarse graining results in single dumbbell model, representing two beads connected through a spring, simplifies the model. From a mathematical viewpoint, the spring represents the restorative force. Depending on the spring's governing force, several interpretations are possible. If the force is linear, the dumbbells are called Hookean. Rouse and Zimm chains are two significant examples of the bead-spring chains with Hookean forces. Examples of a non-linear force are the worm-like chain, Warner or FENE chain (Finitely-Extensible Non-linear Elastic), and Inverse Langevin spring chain.

1.7.2. CONTINUUM LEVEL MODELS

The rheological behavior of polymer molecules is mathematically defined using a constitutive equation in which stress tensor is coupled to the strain rate tensor. The combination of continuity equation, equations of motions, and thermal equations results in a set of differential equations; these provide the mathematical foundation for the fluid's motion at the macroscopic scale. Constitutive equations are usually derived based on kinetic theory principles and the statistical averages (second moments) of polymer conformation distribution within a fluid element.

Closure approximations of the essential variables require developing equations in accordance with the rest of the macroscopic equations, namely conservation of mass, momentum, and energy.

Among the several models describing the rheology of dilute and semi-dilute polymeric solutions, the most popular are Oldroyd-B, UCM (Upper-Convected Maxwell), FENE-P (Finitely Extensible Nonlinear Elastic-Peterlin), FENEP-CR (Finitely Extensible Nonlinear Elastic-Chilcott Rallison, Giesekus, and PTT (Phan-Thein Tanner).

The following section discusses the Oldroyd-B and FENE-P models, which are routinely used for modeling the rheology of dilute polymeric solutions.

1.7.2.1. OLDROYD-B MODEL

There are two approaches to developing this model. In the first, polymer molecules are modeled as non-interacting Hookean elastic dumbbells; the second one originates from continuum mechanics, which is based on the spring-dashpot model, referring to Maxwell model.[15,23]

According to the Maxwell model, Newton's law of viscosity and Hooke's law of elasticity are combined in the following equation:

$$\boldsymbol{\tau} + \lambda \frac{\partial \boldsymbol{\tau}}{\partial t} = -\eta_0 \dot{\boldsymbol{\gamma}} \tag{1}$$

in which $\tau(\tau = \tau_p + \tau_s$ in which τ_s is the stress related to the solvent) , $\dot{\gamma}$, λ and $\eta_0$stand for total stress, rate-of-strain tensor, relaxation time and zero-shear-rate viscosity, respectively.

If in Eq. (1), the partial time derivative is replaced with the upper convected time derivative along with further modification in time constants (details available in[15]), the Oldroyd-B model is derived as follows:

$$\boldsymbol{\tau} + \lambda_1 \boldsymbol{\tau}_{(1)} = -\eta_0 \left(\boldsymbol{\gamma}_{(1)} + \lambda_2 \boldsymbol{\gamma}_{(2)} \right) \tag{2}$$

A variable's upper convected derivative is defined in the following way:

$$\boldsymbol{s}_{(1)} = \frac{\partial \boldsymbol{s}}{\partial t} + \boldsymbol{v}.\nabla \boldsymbol{s} - \ (\nabla \boldsymbol{v})^{\mathrm{T}} \boldsymbol{s} - \boldsymbol{s}.\nabla \boldsymbol{v} \tag{3}$$

In Eq. (2), λ_1 and λ_2 are relaxation time and retardation time, respectively; $\boldsymbol{\gamma}_{(1)}$ and $\boldsymbol{\gamma}_{(2)}$ refer to the first and second rate-of-strain tensors defined elsewhere.[15] There are several modifications to the convected Jeffreys model out of which the "Convected Maxwell Model" has been widely used and is expressed as

$$\boldsymbol{\tau} + \lambda_1 \boldsymbol{\tau}_{(1)} = -\eta_0 \boldsymbol{\gamma}_{(1)} \tag{4}$$

After applying the upper convected derivative and because $\boldsymbol{\gamma}_{(1)} = \dot{\boldsymbol{\gamma}}$ [15], the governing equation is:

$$\boldsymbol{\tau} + \lambda \boldsymbol{\tau}_{(1)} = -\eta_0 \dot{\boldsymbol{\gamma}} \tag{5}$$

The other method for developing the Oldroyd-B model is based on the bead-spring model. If the dumbbell' elastic connector is considered linear, the Hooken spring's governing force will be:

$$\boldsymbol{F}^{(C)} = H\boldsymbol{Q} \tag{6}$$

in which $\boldsymbol{F}^{(C)}$, H and $\boldsymbol{Q}$ are the spring force law, spring constant and dumbbell's end-to-end vector, respectively.[15, 23]

Based on kinetic theory and the different forces acting on the beads in the presence of a solvent (for more details, refer to Bird et al.[15]) in the Hookean dumbbell model, the polymer's contribution to the stress tensor ($\boldsymbol{\tau_p}$) is expressed as Karmers, Eq. (7) and Giesekus , Eq. (8):

$$\boldsymbol{\tau}_p = -nH\langle \boldsymbol{QQ} \rangle + nkT\boldsymbol{\delta} \tag{7}$$

$$\boldsymbol{\tau}_p = +\frac{n\zeta}{4}\langle \boldsymbol{QQ} \rangle_{(1)} \tag{8}$$

In the equations above, n, k, T, ζ, $\langle \boldsymbol{QQ} \rangle$ and $\boldsymbol{\delta}$ are the number of dumbbells per unit volume, Boltzmann constant, temperature, Stokes drag coefficient, the average second moment of the end-to-end vector for the dumbbells and unit tensor, respectively.

Combining Eq. (7) and Eq. (8) by eliminating $\langle \boldsymbol{QQ} \rangle$ from both, leads to the following equation governing the polymer's contribution to the stress tensor:

$$\boldsymbol{\tau}_p + \lambda_H \boldsymbol{\tau}_{p_{(1)}} = -nkT\lambda_H \gamma_{(1)} \tag{9}$$

in which $\lambda_H = \frac{\zeta}{4H}$ is the time constant for the Hookean dumbbells. If Eq. (7) is written in terms of the total stress, $\boldsymbol{\tau}$, Eq. (2) can be recovered.

The Oldroyd-B is a common model used to describe the rheological behavior of highly elastic dilute polymer solutions, known as Boger fluids. These are solutions of high molecular weight polymers in high viscous solvents, such as polyisobutylene in polybutene solvents. The shear viscosity and the first normal stress coefficient of Boger fluids remain constant upon variation of shear rate. The Oldroyd-B model does not predict shear thinning at viscosity or first normal stresses. Therefore, it is an appropriate candidate for describing the rheology of Boger fluids. Nevertheless, predicting infinite extension, which leads to unlimited extensional viscosity, is a major deficiency of this model.

Polymer chains are considered infinitely extensible in the Oldroyd-B model. However, this assumption is unrealistic because polymer chains are stiffened upon signified extension. As a result, the force governing the connector spring is modified, leading to other models, including the FENE-P, explained in the next section.

1.7.2.2. FENE-P MODEL

Based on Eq. (6), in modeling a flexible macromolecule (like a polymer molecule) as a spring, the linear (Hookean) relationship is applicable for small extensions; however, as the polymer molecule extends, it becomes stiffer; because this means the spring cannot be stretched beyond a certain limit of separation referred to as Q_0. The spring force law is given as

$$\boldsymbol{F}^{(C)} = \frac{H\boldsymbol{Q}}{1 - \left(\frac{Q}{Q_0}\right)^2} \qquad Q \leq Q_0 \tag{10}$$

Thus, contrary to Eq. (6), this relationship is nonlinear.

For the finitely extensible nonlinear elastic (FENE) dumbbells, two time constants are defined. The first is λ_H, the same as for the Hookean dumbbells; the second is the time constant for rigid dumbbells λ_Q:

$$\lambda_Q = \frac{\zeta Q_0^2}{12kT} \tag{11}$$

Two time constants λ_H and λ_Q can be combined to create a dimensionless ratio, b, which represents the extensibility of polymer molecule:

$$b = \frac{3\lambda_Q}{\lambda_H} \tag{12}$$

If b goes to infinity, the Hookean dumbbell is recovered.

For this kind of non-Hookean dumbbell model, the polymer contribution to the stress tensor is defined via Karmers, Eq. (13) and Giesekus, Eq. (14):

$$\boldsymbol{\tau}_p = -nH\left\langle \frac{\boldsymbol{QQ}}{1-\left(\frac{Q}{Q_0}\right)^2} \right\rangle + nkT\boldsymbol{\delta} \tag{13}$$

$$\boldsymbol{\tau}_p = +\frac{n\zeta}{4}\langle \boldsymbol{QQ} \rangle_{(1)} \tag{14}$$

Eliminating $\langle \boldsymbol{QQ} \rangle$ from these equations requires mathematical approximations for the average values in the above equations. The primary approximation is applied to the first term of Eq. (13) in the following way:

$$\left\langle \frac{\boldsymbol{QQ}}{1-\left(\frac{\boldsymbol{Q}}{\boldsymbol{Q}_0}\right)^2} \right\rangle = \frac{\langle \boldsymbol{QQ} \rangle}{1-\left\langle \frac{Q^1}{Q_0^2} \right\rangle} + \varepsilon Q_0^2 \boldsymbol{\delta} \tag{15}$$

where ε is defined as

$$\varepsilon = \frac{2}{b(b+2)} \tag{16}$$

After some manipulations,[15] the following equation is derived:

$$Z\boldsymbol{\tau}_p + \lambda_H \boldsymbol{\tau}_{p(1)} - \lambda_H \left[\boldsymbol{\tau}_p - (1-\varepsilon b) nkT\boldsymbol{\delta}\right] \frac{D\, ln\, Z}{Dt} = -(1-\varepsilon b) nkT \lambda_H \gamma_{(1)} \qquad (17)$$

in which Z is defined as

$$Z = 1 + \frac{3}{b}\left((1-\varepsilon b) - \frac{tr\boldsymbol{\tau}_p}{3nkT}\right)$$

Note that in the primary approximation as shown in Eq. (15), if the second term is negligible, the approximation is called Peterlin's approximation, leading to the Finitely Extensible Nonlinear Elastic-Peterlin (FENE-P) model. The reformulation of the FENE-P model based on a similar definition of extensibility described above will be given in the next chapter. As will be seen, L^2 will be used as an alternative for b holding the same definition of extensibility.

CHAPTER 2
LITERATURE RIVIEW

2.1. BRIEF HISTORY OF TAYLOR-COUETTE VISCOELASTIC INSTABILITIES

Giesekus[5] first observed purely elastic instability in the viscoelastic Taylor-Couette flow. Since then, several works on viscoelastic instabilities of flow systems with curved streamlines have established. As mentioned earlier, the Taylor-Couette system has been the flow of interest.

The elasticity number $E = De/Re$, is commonly used in characterizing viscoelastic instabilities. E is solely dependent on fluid properties and is independent of the flow. Hence, the purely elastic region is defined as $E \to \infty$. In 1989, Muller and coworkers, observed a purely elastic instability in the Taylor-Couette flow of a non-shear-thinning dilute polymeric solution called a Boger fluid.[6] The same researchers predicted similar purely elastic instabilities by implementing a linear stability analysis for the same type of viscoelastic flow system.[7] The instability's mechanism can be attributed to the adverse gradient of elastic hoop stress across the curved streamlines. The polymer molecules are stretched in primary shear flow leading to elastic stress build-up. In turn, the primary shear flow is destabilized at $O(1)$ De and a secondary flow composed of toroidal vortices stacked along the axes of the cylinder is realized. In previous works, the Taylor-Couette flow's stability behavior has been investigated using dilute solutions of high molecular weight polymers, e.g., polyisobuthylene (PIB) in highly viscous solvents of low molecular weight[7,9,10,11,24,25] or high molecular weight polyacrylamide (PAA) in viscous sugar syrup.[17,26,27] Use of Boger fluids allows the elimination of the fluids' shear-

thinning behavior in the experiment because Boger fluids show constant first normal stress coefficients and viscosity over a wide range of shear rates. The Oldroyd-B model with a single relaxation time λ and a parameter β as the ratio of solvent to total solution viscosity has been widely used to qualitatively describe the rheological behavior of Boger fluids.[7,8,18,19,20,28,29,30]

2.2. DISCREPANCIES IN EXPERIMENTAL AND NUMERICAL STUDIES

The first observed instability modes, either in experimental or numerical works, were referred to as elastic instabilities.[5,6,7,8,9,10,28,29] However, stheoretical predictions and experimental observation[24,25,28,29] and experimental observations[7,24,25] alone have revealed qualitative and quantitative disparities.

The critical Deborah value observed at flow transitions in Baumert and Muller's[24] experimental investigation is an order of magnitude lower than the ones predicted in experiments by Muller et al.[10], Larson et al.[7], and Shaqfeh et al.[11]. For example, while in Larson and his coworkers' experiments[6], a time-dependent secondary vortex flow with an onset critical Deborah number of 16 ($\beta = 0.79$, ratio of cylinder radii $\delta = 0.87$) is observed, Baumert and Muller's experimental investigations dealing with $\beta = 0.79$ and the ratio of cylinder radii $\delta = 0.87$ show steady and axisymmetric toroidal vortices at the critical Deborah number of 1.5.[24,25] In addition to the observed instability's modes disparities, the critical Decorah number reported in Baumert and Muller's work is an order of magnitude lower than that reported by Larson et al.[7] Moreover, in contrast to results observed in Baumert and Muller's experiment, the viscoelastic Taylor-Couette flow's linear stability analysis predicts non-axisymmetric and time-dependent instability

modes.[28] Additionally, Groisman et al.'s experiments confirm Muller et al.'s previous observations, i.e. primary instability transitions occur as a stationary and axisymmetric vortex flow reminiscent of the Taylor vortices observed in the Newtonian case.[26] Baumert and Muller showed that time-dependent and non-axisymmetric flow patterns manifest only as higher order transitions. Furthermore, Avgousti and Beris[29] showed that a secondary flow transition occurs through a subcritical bifurcation, implying that neither of the two secondary flow patterns, i.e. spirals (tilted vortices spanning the gap and axially travelling) and ribbons (vortices spanning and oscillating both in time and azimuthal position) are stable. It has been indicated that the base flow's spatio-temporal symmetries dictate the bifurcation to be degenerate,[4] i.e. there is a hysteresis in the flow pattern dynamic that linear stability analysis cannot predict. Following Avgousti and Beris work, nonlinear stability analysis was implemented in two different works by Sureshkumar et al and Renardy et al.[30,31] Furthermore, Renardy et al.[31] have shown that for relatively narrow gaps at least one of the two degenerate bifurcations is subcritical, implying that in accordance with the base flow's symmetries, neither ribbons nor spirals are stable modes. In the same work, the bifurcation for relatively large gaps has been shown to be supercritical indicating that only one of the aforementioned secondary flows is stable.[30,31]

Several interpretations have been proposed to explain disparities observed between experimental observations and theoretical prediction. First, despite Boger fluids' non-shear-thinning behavior in the presence of a shear field, the fluids' response to extensional deformations and transient shear is complicated, mandating the use of more

sophisticated constitutive models to capture the rheological behavior. These models must encompass the spectrum of relaxation time and the Boger fluids' non-linear viscoelasticity rather than being confined to the single-mode Oldroyd-B model. Recently, the multi-mode Oldroyd-B (MMO-B) and multimode Giesekus (MMG) models have been used for the flow systems of cone-and-plate and parallel-plate.[32] Al-Mubaiyedh et al.[33] have applied both models to the Taylor-Couette flow. Much like the single-model Oldroyd-B model, the MMO-B and MMG models predict non-axisymmetric and time-dependent secondary flow patterns.

Therefore, it can be deduced that discrepancies among several reports on the viscoelastic Taylor-Couette flow's instability patterns cannot be explained by considering the relaxation spectrum or nonlinear viscoelasticity. Subsequently, energetics' influence on the stability behavior of the viscoelastic Taylor-Couette flow was investigated. Because of both the very high viscosity of Boger fluids used in previous experiments at room temperature ($O(1)Pa.s$) and the large activation energy attributed to the viscosity and relaxation time ($O(10^2)KJ/mol$)[34] when such fluids are subjected to a shear field flow, significant heat generation is associated with the viscous dissipation. Considering such characteristics, even a temperature variation of 1-2°C across the gap can considerably modify the instability onset conditions, specifically reducing the critical shear rate. It is noteworthy that instabilities such as thermo-elastic instabilities are observed in other viscoelastic flow systems with different curvilinearity, such as the Dean flow (or pressure-driven flow through channels) and the cone-and-plate flow.[35,36]

Al-Mubaiyedh et al. applied a thermodynamically consistent formulation of the Oldroyd-B model to evaluate thermal effects on the hydrodynamic stability of viscoelastic Taylor-Couette flow;[18,19,20] their results revealed a symmetric and time-invariant instability mode, which is consistent with the instability flow patterns that Baumert and Muller observed.[24,25] This new mode appears due to the coupling of viscous dissipation with thermal sensitivity of high viscous dilute polymeric solution; this coupling gives rise to convection of the base state temperature gradient by the radial perturbation velocity leading to a critical Deborah number with an order of magnitude lower than that of the corresponding isothermal flow. Furthermore, the nonlinear stability analysis that Al-Mubaiyedh et al. implemented showed that the bifurcation corresponding to such thermo-elastic instability is supercritical, i.e. in a flow with the vanishing Reynolds number, the bifurcation leads to the axisymmetric and time-independent toroidal vortices resembling Taylor vortices.[20]

While much effort was focused on resolving this aforementioned discrepancy, several experimental studies were performed on higher order non-linear flow transitions in the Taylor-Couette flow in the past decade. Specifically, Groisman and Steinberg (1996, 1997, 1998) observed three dominant flow patterns in dilute PAAm aqueous solutions at high Wi and $O(1)$ elasticity number, $E = Wi/Re$, namely, diwhirls (DW), oscillatory strips (OS) and disordered states (DO).[26,37,38] Subsequently, these flow patterns were reproduced via hi-fidelity direct numerical simulations (DNS) (Thomas, Sureshkumar and Khomami 2006; Thomas, Khomami and Sureshkumar 2009), i.e. the

Wi and E corresoiding to transition from one flow state to another were faithfully reproduced.[13,14]

Recently, Steinberg and his coworkers observed the critical Weissenberg number (often used interchangeably with the Deborah number) where an abrupt transition occurs resulting in a high-order flow pattern transition named, "elastic turbulence" characterized by broad ranges of spatial and temporal scales.[17] Referring to Fig. 18 in their work, the first linear instability transition occurs at Deborah number of 1. However, the influence of energetics has not been discussed. In these researchers' experiments, the solution of Polyacrylamide (PAA) with high molecular weight of $18{,}000{,}000(\frac{gr}{grmol})$ in a highly viscous solvent of sugar and NaCl in water is considered a Boger fluid. Such Boger fluids are prone to manifest viscous dissipation when subjected to a shear field. Therefore, the lack of information on thermal effects necessitates evaluating the thermal effects to get deeper insight into the instability conditions.

2.3. GOAL OF OUR STUDY

In the current study, the onset conditions for purely elastic and thermoelastic instabilities in the Taylor-Couette flow over a wide gap ratio and fluid thermal sensitivity is studied. This is accomplished via performing linear stability analysis with set of continuum conservation and constitutive equations. Specifically, the Oldroyd-B and the FENE-P constitutive models have been used to describe the rheological characteristics of dilute polymeric solutions. A comprehensive analysis has clearly shown that although De for the onset of instability is observed as the gap ratio is enhanced, without considering thermal effects an $O(1)$ De cannot be realized. These findings doubt as existence of

purely elastic turbulence in Taylor-Couette flows at $O(1)$ as reported by Groisman and Stienberg.[17]

CHAPTER 3
PROBLEM FORMULATION

3.1. GOVERNING EQUATIONS

Fluid motion between two infinitely long and concentric cylinders of radii, R_1 and $R_2(R_1 < R_2)$, is considered (as shown in Fig. 1); the inner cylinder rotates with angular velocity of Ω_1 and outer cylinder is stationary. The total solution viscosity, density and the polymer solution's average relaxation time are noted as η_T, ρ and λ, respectively. The total solution viscosity is the sum of the solvent viscosity and polymeric contributions as expressed in $\eta_T = \eta_S + \eta_{P,}$ where η_S and η_P refer to the solvent viscosity and polymeric viscosity, respectively.

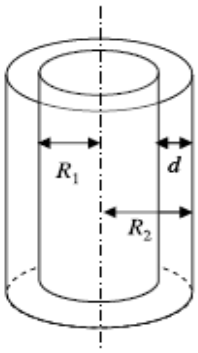


Figure 1 Schematic of the Taylor-Couette flow geometry

Macroscopically, viscoelastic flow problems are solved by combining the constitutive equation with the equations of mass, momentum, and energy conservation expressed as

$$\nabla . v = 0 \tag{18}$$

$$\rho\left(\frac{\partial v}{\partial t} + v.\nabla v\right) = -\nabla P + \eta_s \nabla^2 v + \nabla . \tau_p \tag{19}$$

$$\rho C_p \left(\frac{\partial T}{\partial T} + v\,.\nabla T\right) = k\nabla^2 T + \eta_s \dot{\gamma} : \dot{\gamma} + \tau_p : \nabla v \tag{20}$$

In these equations, P and v represent hydrodynamic pressure and the flow velocity, respectively; τ_p is the polymeric contribution to the stress

To non-dimensionalize the governing equations, the gap width, $d = R_2 - R_1$, $d/R_1\Omega_1$, $R_1\Omega_1$, $\rho(R_1\Omega_1)^2$ and $\eta_P R_1\Omega_1/d$ are chosen as the non-dimensionalizing scales for length, time, velocity, pressure, and polymeric stress, respectively. Additionally, the temperature is scaled with a reference temperature of T_0. In the flow system, the temperature difference is considered to be within the order of $O(1℃)$ across the gap width, which is attributed to heat generation induced by viscous dissipation. Considering these conditions (Note that P , $\boldsymbol{v}$, $\boldsymbol{\tau}_p$,r and T used in the following equations, are all dimensionless), the fluid is practically incompressible, leading to the following equation of continuity:

$$\nabla . \boldsymbol{v} = 0 \tag{23}$$

The non-dimensionalized equation of motion is expressed as

$$\left(\frac{\partial \boldsymbol{v}}{\partial t} + \boldsymbol{v}.\nabla \boldsymbol{v}\right) = -\nabla P + \frac{1}{Re}\nabla . \{\beta\, e^{\epsilon_s\left(\frac{1}{T}-1\right)}(\nabla \boldsymbol{v} + (\nabla \boldsymbol{v})^{\mathrm{T}}) + (1-\beta)\frac{1}{De}\,\boldsymbol{\tau}_p \tag{24}$$

where β is the ratio of solvent to total viscosity at the reference temperature, and $\beta = \eta_s/\eta_T$, ϵ_s is dimensionless activation energy defined as

$$\epsilon_s = \frac{\Delta H_s}{RT_0^*} \tag{25}$$

In this equation, ΔH_s and R are activation energy and universal gas constant, respectively. In Eq. (24) , $\nabla \boldsymbol{v} + (\nabla \boldsymbol{v})^T$ is defined as $\kappa = \nabla \boldsymbol{v} + (\nabla \boldsymbol{v})^T$, the rate of deformation tensor. In the same equation, the dimensionless Reynolds number appears as Re which is defined as

$$Re = \frac{\rho R_1 \Omega_1 d}{\eta_T} \tag{26}$$

In the Oldroyd-B model, polymer molecules are modeled as non-interacting elastic dumbbells in the case of the linear (Hookean) spring connector. The polymeric stress is formulated as the departure of the conformation tensor, $\boldsymbol{C}$, representing the ensemble average of the second moment of the polymer chain's end-to-end vector from its equilibrium conformation denoted as isotropic unit tensor I,

$$\boldsymbol{\tau}_p = \frac{\boldsymbol{C} - \boldsymbol{I}}{De} \tag{27}$$

in which $\boldsymbol{C}$, is non-dimensionalized with respect to a characteristic dumbbell length defined in terms of kT/H. Here k, T and H correspond to the Boltzmann constant, temperature and Hookean spring constant, respectively.

Using the principle of time temperature superposition and the concept of pseudo time[21] the isothermal Oldroyd-B constitutive equation for polymeric stress can be modified in a the thermodynamically consistent fashion for the influence of thermal history on the stress and is given by

$$\boldsymbol{\tau}_p + De.\, e^{\epsilon_\lambda\left(\frac{1}{T}-1\right)}[\boldsymbol{\tau}_{p(1)} - (\frac{\partial}{\partial t}(\ln T) + \boldsymbol{v}.\nabla \ln T)\boldsymbol{\tau}] = 2e^{\epsilon_p\left(\frac{1}{T}-1\right)}(\nabla \boldsymbol{v} + (\nabla \boldsymbol{v})^{\mathrm{T}}) \tag{28}$$

where $\boldsymbol{\tau}_{p(1)}$ is the upper convected derivative defined as

$$\boldsymbol{\tau}_{p(1)} = \frac{\partial \boldsymbol{\tau}_p}{\partial t} + \boldsymbol{v}.\nabla\boldsymbol{\tau}_p - (\nabla \boldsymbol{v})^{\mathrm{T}}\boldsymbol{\tau}_p - \boldsymbol{\tau}_p.\nabla \boldsymbol{v} \tag{29}$$

ε_λ and ε_p are the dimensionless activation energies for the relaxation time and polymer viscosity, respectively noted as

$$\epsilon_p = \frac{\Delta H_p}{RT_0^*} \;\; and \;\; \epsilon_\lambda = \frac{\Delta H_\lambda}{RT_0^*} \tag{30}$$

In Eq. (28) the dimensionless number, De known as the Deborah number, represents the ratio of polymer relaxation time to the characteristic flow time scale and is defined as

$$De = \frac{\lambda R_1 \Omega_1}{d} \tag{31}$$

Whereas inter-molecular forces of polymer molecules governed by linear elastic spring force lead to the Oldroyd-B model, modeling the polymer molecules as finitely extensible dumbbells with non-linear (non-Hookean) elastic spring forces results in the FENE-P model. In this case, the viscoelastic stress is macroscopically related to the conformation tensor as[39,40]

$$\boldsymbol{\tau}_p = \frac{f(\boldsymbol{C})\boldsymbol{C} - \boldsymbol{I}}{De} \tag{32}$$

In this equation, $f(\boldsymbol{C})$ is known as the Peterlin function, which is defined as

$$f(\boldsymbol{C}) = \frac{L^2 - 3}{L^2 - trace(\boldsymbol{C})} \tag{33}$$

where L refers to the polymer chain's maximum extensibility, i.e. of the dumbbell end-to-end distance vector. Note that L^2 is an alternative representative for the parameter b defined in chapter 2.

The evolution equation based on conformation tensor is

$$e^{\epsilon_\lambda\left(\frac{1}{T}-1\right)}\left[\frac{D}{Dt}\ln f(\boldsymbol{C}).\boldsymbol{C}+\boldsymbol{C}_{(1)}-\frac{1}{f(\boldsymbol{C})}-\frac{D}{Dt}\ln T.(f(\boldsymbol{C})\boldsymbol{C}-\boldsymbol{I})\right] + \frac{L^2}{L^2-3}\left(\frac{f(\boldsymbol{C})\boldsymbol{C}-\boldsymbol{I}}{De}\right)=\left(e^{\epsilon_p\left(\frac{1}{T}-1\right)}-e^{\epsilon_\lambda\left(\frac{1}{T}-1\right)}\right)(\nabla\boldsymbol{v}+(\nabla\boldsymbol{v})^T) \quad (34)$$

in which $\frac{D}{Dt}$ is defined as the convective derivative in the following manner:

$$\frac{D}{Dt}S=\frac{\partial}{\partial t}S+v.\nabla\ln S \quad (35)$$

While the Oldroyd-B model, i.e. recovered from above by setting $(\boldsymbol{C})=\mathbf{1}$, predicts no shear-thinning behavior for the polymer solution, the FENE-P model exhibits shear-thinning both for shear viscosity and the first normal stress coefficient. Moreover, the zero shear viscosity for the FENE-P and Oldroyd-B models are given as follows:

$$\eta_{Oldroyd-B}=\frac{n\zeta kT^*}{2H} \quad (36)$$

$$\eta_{FENE-P}=\frac{n\zeta kT^*}{2H}\left(1-\frac{3}{L^2}\right) \quad (37)$$

where n, ζ, k and H are the number of dumbbells in the volume unit, Stokes drag coefficient, Boltzmann constant, the absolute temperature, and spring constant.[15,23] Eq. (37) shows that the viscosity predicted by the FENE-P model at zero shear rate is dependent on the polymer chain's extensibility. At the limit of $L \to \infty$, two rheological models will produce similar results for shear viscosity.

The combination of the viscoelastic fluid's thermal sensitivity and viscous heating are regarded as the dominant thermal effects. Subjected to shear flow, the viscoelastic fluid experiences viscous dissipation leading to heat generation. The energy equation is expressed as

$$Pe\left(\frac{\partial T}{\partial t}+\boldsymbol{v}.\nabla T\right)=\nabla^2 T+Br\left[\frac{\beta}{2}e^{\epsilon_s\left(\frac{1}{T}-1\right)}(\nabla\boldsymbol{v}+(\nabla\boldsymbol{v})^T):(\nabla\boldsymbol{v}+(\nabla\boldsymbol{v})^T)+(1-\beta)(\boldsymbol{\tau}:\nabla\boldsymbol{v})\right] \quad (38)$$

where Peclet number, Pe, and Brinkman number, Br, are defined as

$$Pe=\frac{\rho C_p R_1\Omega_1 d}{K} \quad (39)$$

$$Br=\frac{\eta(R_1\Omega_1)^2}{kT_0^*} \quad (40)$$

Here C_p and K are the specific heat capacity at constant pressure and thermal conductivity, respectively. Note that fluid properties are evaluated at T_0 . Pe demonstrates the ratio of convective heat flux to conductive heat flux, and Br represents the ratio of viscous heat to conductive heat flux. Typically, Pe and Br have the order of magnitude $O(10^5)$ and $O(10^{-2})$ for the Boger fluids used in Taylor-Couette experiments.[24,25] An important parameter representing the thermal sensitivity of fluids is the Nahme-Griffith number, Na, defined as

$$Na=\frac{|\partial\eta/\partial T^*|_{T_0^*}(R_1\Omega_1)^2}{k}=\left(\beta\varepsilon_s+(1-\beta)\varepsilon_p\right)Br \quad (41)$$

Note that the magnitude of Na is $O(1)$ for small values of Br in the case of thermally sensitive fluids (ε_s and $\varepsilon_p \gg 1$).

The complementary part of the problem set-up is the boundary conditions at the cylinder walls. For the velocity, the dynamic condition at both of the walls are taken as no-slip conditions,[41] leading to the following type of equations.

$$\boldsymbol{v}=e_\theta \quad at \quad r=r_1 \quad (42a)$$

$$\boldsymbol{v}=\frac{R_2\Omega_2}{R_1\Omega_1}e_\theta \quad at \quad r=r_2 \quad (42b)$$

On the other hand, to simulate typical experimental conditions,[24,25] the Neumann boundary condition's experiments have been used as stated below:

$$\frac{\partial T}{\partial r} = 0 \quad at \quad r = r_1 \tag{43a}$$

$$-\frac{\partial T}{\partial r} = Bi(T - T_\infty) \ at \quad r = r_2 \tag{43b}$$

In Eq. 43b, Bi represents the heat lost by convection to the surrounding medium defined as

$$Bi = \frac{hd}{k} \tag{44}$$

and T_∞denotes the dimensionless ambient temperature.

3.2. LINEAR STABILITY ANALYSIS AND NUMERICAL IMPLEMENTATION

Linear stability analysis (LSA) is applied to scrutinize the onset of instabilities in isothermal and non-isothermal Taylor-Couette flow. Additionally, this method provides information about the secondary flow's spatio-temporal characteristics.

In this method, the stability threshold is predicted via the normal mode perturbation analysis in which infinitesimally small disturbances are superimposed onto the base state flow solution $\boldsymbol{u}_{ss} \equiv (P, \boldsymbol{v}_r, \boldsymbol{v}_\theta, \boldsymbol{v}_z, \boldsymbol{C}_{rr}, \boldsymbol{C}_{r\theta}, \boldsymbol{C}_{rz}, \boldsymbol{C}_{\theta\theta}, \boldsymbol{C}_{\theta z}, \boldsymbol{C}_{zz}, T)$ which is mathematically expressed as

$$\boldsymbol{u} = \boldsymbol{u}_{ss} + \hat{\boldsymbol{u}}(r) e^{i\alpha z + i\xi\theta + \sigma i} \tag{45}$$

where $i = \sqrt{-1}$ and σ is the complex eigenvalue defined as $\sigma = \sigma_r + \sigma_i i$. σ_r and σ_i correspond to the real and imaginary parts of the complex eigenvalue, respectively. σ_r shows the decay or growth rate of the perturbation while σ_i stands for the perturbation's temporal frequency. $\hat{\boldsymbol{u}}(r)$ is the perturbation functions' complex infinitesimal amplitude

vector. Moreover, in Eq. (21) α and ξ are the assumed periodicity's dimensionless wave numbers in directions of z and θ, respectively, which can only have integer and non-negative values.

Substitution of Eq. (21) into the Eqs. (23),(24),(32),(34) and (38) and linearization about the steady state solution lead to a complex generalized differential eigenvalue problem (DEVP) of the following ordinary differential equation:

$$A\hat{\boldsymbol{u}} = \sigma B\hat{\boldsymbol{u}} \tag{46}$$

in which A and B are linear operators encompassing the spatial and temporal information resulting from the linearization about the steady state solution and $\hat{\boldsymbol{u}}$ is the dependent variables ($P, \boldsymbol{v}_r, \boldsymbol{v}_\theta, \boldsymbol{v}_z, \boldsymbol{C}_{rr}, \boldsymbol{C}_{r\theta}, \boldsymbol{C}_{rz}, \boldsymbol{C}_{\theta\theta}, \boldsymbol{C}_{\theta z}, \boldsymbol{C}_{zz}, T$).

A Chebyshev pseudo-spectral collocation method is applied to numerically solve the DEVP set of equations; this method is explained in detail elsewhere.[29,30,31,42,43] addition, the nonlinear non-isothermal base flow equations have been solved using a Chebyshev spectral method.

CHAPTER 4
RESULTS AND DISCUSSION

4.1. CHOICE OF PARAMETERS AND STEADY-STATE SOLUTION

Based on experiments by Steinberg et al[17], the ratio of radii is $\varepsilon = d/R_1 = 0.5$ equivalent to $\delta = R_2/R_1 = 0.66$. In their study, the outer cylinder is stationary, $\Omega_2 = 0$ and surrounded by a thermal jacket with a square cross-section made out of Plexiglass to control the temperature. In the same experiments, the fluid properties are $\eta_p = 0.1$ Pas, $\eta_s = 0.32$ Pas $(\beta = 0.765)$ and $\lambda = 3.4$ s measured at 12℃ for the Polyacrylamide(PAA)m dilute solutions. Additionally, as mentioned in Quinzani et al. [34] work, fluid properties are $\eta_p = 5.65$ Pas, $\eta_s = 8.12$ Pas $(\beta = 0.57)$ and $\lambda = 0.793$ s measured at 25℃. The fluids used in Ref. 17 and 34 are referred to as fluids 1 and 2, respectively.

Motivated by the experimental work of Steinberg et al.,[17] and the resemblance between rheological and thermal properties of their Boger fluid and those used by Quinzani et al, i.e. PAAm solution in NaCl/saccharose water solvent (fluid 1), and Polyisobuthylene (PIB)/Polybutene(PB)/Tetradecane(C14) (fluid 2), we use the same activation energies for the PAAm solution as the PIB/PB/(C14) solution.[17,34] Specifically, the activation energy associated with the shear viscosity and relaxation time are $\Delta H_P/R = \Delta H_\lambda/R = 7362K$. Also, the activation energy associated with the solvent is $\Delta H_S/R = 7432K$. Furthermore, the temperature outside the outer cylinder is assumed to deviate ± 1℃ from the reference temperature ($T_0 = 285°K$).

The base state solution has been calculated utilizing steady state equations of motion, constitutive equations, and the energy equation. Here, however, only equations based on the FENE-P model are given.

$$\beta\left(\frac{-\partial T}{\partial r}\right)\left(\frac{1}{T^2}\right)e^{\varepsilon_s\left(\frac{1}{T}-1\right)}\left(\frac{\partial \boldsymbol{v}_\theta}{\partial r}-\frac{\boldsymbol{v}_\theta}{r}\right)+\beta e^{\varepsilon_s\left(\frac{1}{T}-1\right)}\left(\frac{\partial^2 \boldsymbol{v}_\theta}{\partial r^2}+\frac{1}{r}\frac{\partial \boldsymbol{v}_\theta}{\partial r}+(-\frac{1}{r^2}\boldsymbol{v}_\theta)\right)$$
$$+\left(\frac{1}{De}\right)(1-\beta)\left(\frac{\frac{\partial \boldsymbol{C}_{rr}}{\partial r}+\frac{\partial \boldsymbol{C}_{\theta\theta}}{\partial r}+\frac{\partial \boldsymbol{C}_{zz}}{\partial r}}{(L^2-[\boldsymbol{C}_{rr}+\boldsymbol{C}_{\theta\theta}+\boldsymbol{C}_{zz}])^2}(L^2-3)\boldsymbol{C}_{r\theta}+\frac{\partial \boldsymbol{C}_{r\theta}}{\partial r}.f(\boldsymbol{C})\right.$$
$$\left.+\frac{2}{r}f(\boldsymbol{C})\boldsymbol{C}_{r\theta}\right)=0 \tag{47}$$

$$\boldsymbol{C}_{rr}-\frac{1}{f(\boldsymbol{C})}=0 \tag{48}$$

$$\boldsymbol{C}_{r\theta}-De\boldsymbol{C}_{rr}e^{\varepsilon_\lambda\left(\frac{1}{T}-1\right)}\left(\frac{L^2-[\boldsymbol{C}_{rr}+\boldsymbol{C}_{\theta\theta}+\boldsymbol{C}_{zz}]}{L^2}\right)\left(-\frac{\boldsymbol{v}_\theta}{r}+\frac{\partial \boldsymbol{v}_\theta}{\partial r}\right)=0 \tag{49}$$

$$\boldsymbol{C}_{\theta\theta}-2De\boldsymbol{C}_{r\theta}e^{\varepsilon_\lambda\left(\frac{1}{T}-1\right)}\left(\frac{(L^2-[\boldsymbol{C}_{rr}+\boldsymbol{C}_{\theta\theta}+\boldsymbol{C}_{zz}])}{(L^2)}\right)\left(-\frac{\boldsymbol{v}_\theta}{r}+\frac{\partial \boldsymbol{v}_\theta}{\partial r}\right)$$
$$-\frac{(L^2-[\boldsymbol{C}_{rr}+\boldsymbol{C}_{\theta\theta}+\boldsymbol{C}_{zz}])}{(L^2-3)}=0 \tag{50}$$

Moreover, the heat transfer phenomenon is supposed to be fully developed from a thermal viewpoint. Increasing the Pe number leads to the time-scale increment associated with the development of the steady-state temperature profile. Based on this information, the energy equation in terms of the conformation tensor is represented as

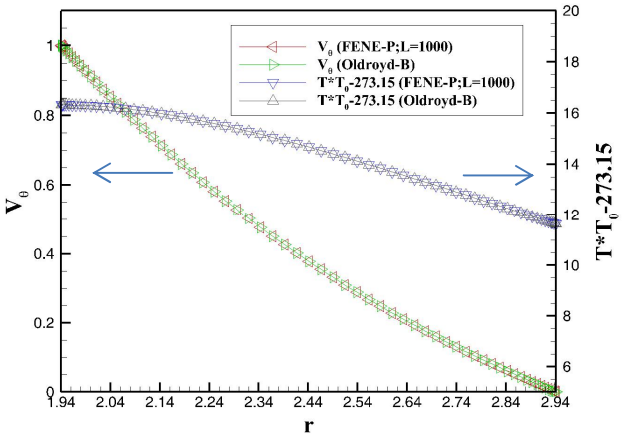
$$\frac{1}{r}\frac{\partial T}{\partial r}+\frac{\partial^2 T}{\partial r^2}+Br\left(\beta e^{\varepsilon_s\left(\frac{1}{T}-1\right)}\left(\frac{-\boldsymbol{v}_\theta}{r}+\frac{\partial \boldsymbol{v}_\theta}{\partial r}\right)^2+(1-\beta)\frac{1}{De}\boldsymbol{C}_{r\theta}.f(\boldsymbol{C})\left(\frac{-\boldsymbol{v}_\theta}{r}+\frac{\partial \boldsymbol{v}_\theta}{\partial r}\right)\right)$$
$$=0 \tag{51}$$

As can be deduced, equations (47)-(51) along with (42)-(43) constitute a nonlinear boundary value problem, which was solved by a Chebyshev spectral technique.

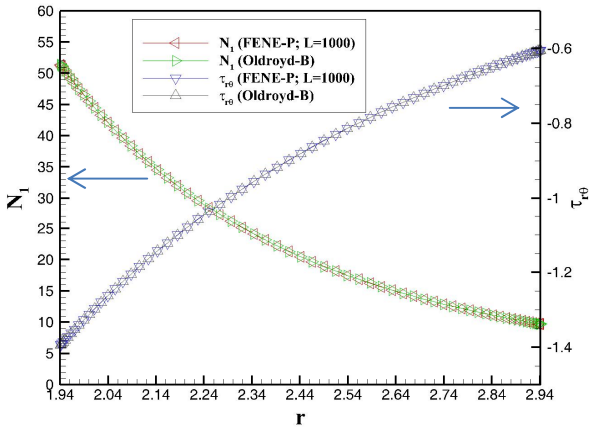
In Fig. 2, the steady-state profiles using the rheological properties and geometrical parameters used in Ref. 17 are depicted. In this figure, the results obtained using the Oldroyd-B model are compared those results attained using the FENE-P model. As can be observed, when L is set to 1000 (a relatively high value of the maximum extensibility), both models produce the same results. As formerly explained, the Oldroyd-B model is considered to be the specific case of FENE-P where the polymer chains are assumed to be infinitely extensible.

The base flow profiles for temperature and gradient of temperature, the azimuthal velocity and gradient of azimuthal velocity, and the shear stress and first normal stress are depicted as shown in Fig. 3. As expected, with increased De leads to a higher first normal stress. Normal stresses arising within the Taylor-Couette flow system are attributed to the fluid's elasticity. Thus, higher Deborah values strengthen the normal stresses across the curvilinear streamlines. Nevertheless, the shear stress profile is independent of the De number. According to the shear stress's steady state value demonstrated in Eq. (52), the azimuthal velocity's gradient determines the shear stress value.

$$\boldsymbol{\tau}_{r\theta} = e^{\varepsilon_\lambda\left(\frac{1}{T}-1\right)}\left(\frac{L^2-3}{L^2}\right)\left(\frac{-\boldsymbol{v}_\theta}{r}+\frac{\partial \boldsymbol{v}_\theta}{\partial r}\right) \tag{52}$$



(a)

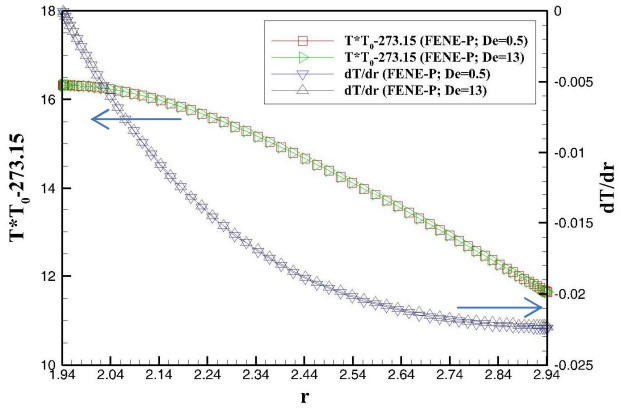


(b)

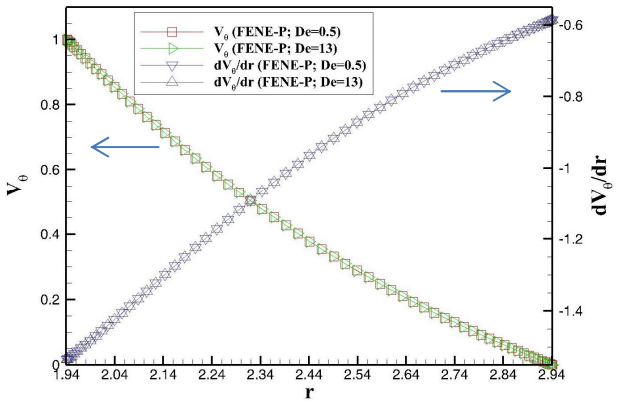
Figure 2 Comparison of base state solution for Oldroyd-B and FENE-P models at De=13, Bi=10, Br=0.0244, Pe=20000, β=0.765, ε=0.5 (a) V_θ and T^*T_0-273.15℃ and (b) $\tau_{r\theta}$ (shear stress) and N_1 (first normal stress)

For both low and high Deborah values, the variation in the velocity gradient's profiles is negligible. The same scenario is observed for the temperature gradient.

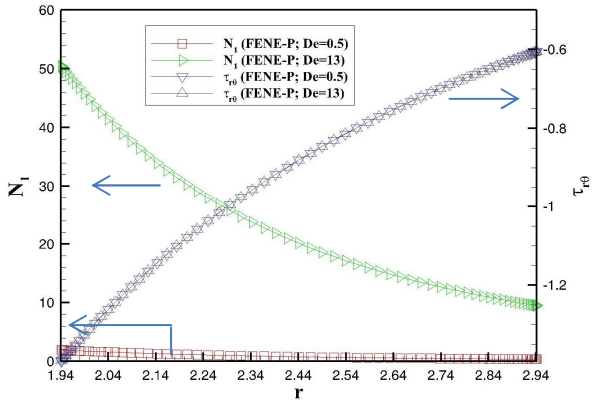
The steady state profiles across the gap are represented as a function of De and L as shown in Fig. 4 and Fig. 5.



(a)



(b)



(c)

Figure 3 Steady state profiles for *Bi*=10, *Br*=0.0244, *Pe*=20000, β=0.765, *L*=1000, ε=0.5 at *De*=0.5 and *De*=13 (a) and T^*T_0-273.15℃ (b) V_θ and dV_θ/dr (c) N_1 and $\tau_{r\theta}$

Referring to Figures 4c-d and 5c-d, at a fixed radial position, the shear stress and normal stress tend to increase at higher extensibilities for both cases, $De = 0.5$ and $De = 13$ (corresponding to stationary/symmetric and oscillatory/asymmetric instability modes, respectively, as shown later). At a fixed radial position, higher shear stress values are expectable at higher extensibilities if Eq. (52) is considered which expresses the shear stress steady state value. Similar conclusion is made if the mathematical expression of first normal stress is considered.

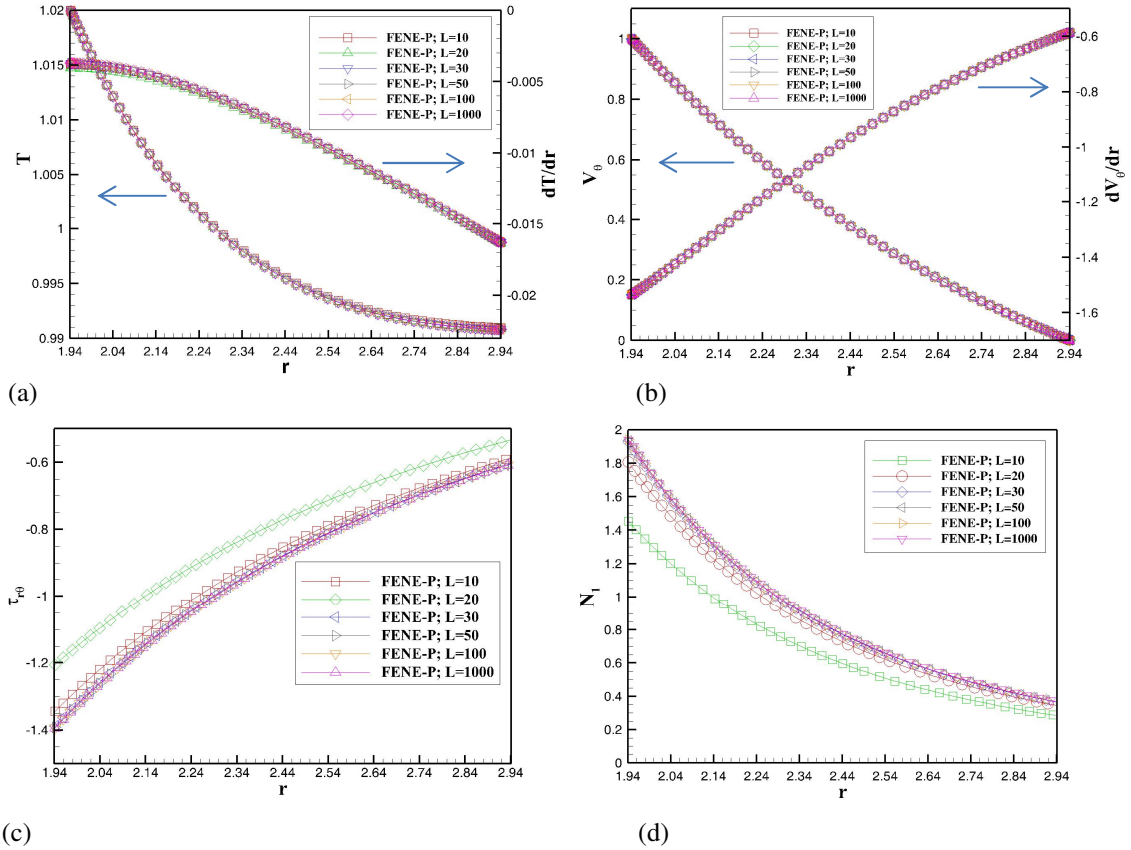


Figure 4 Steady state profiles calculated for Bi=10, Br=0.0244, Pe=20000, β=0.765, ε=0.5 at De=0.5 (a) T^*T_0-273.15℃ (b) V_θ and dV_θ/dr (c) $\tau_{r\theta}$ (d) N_1

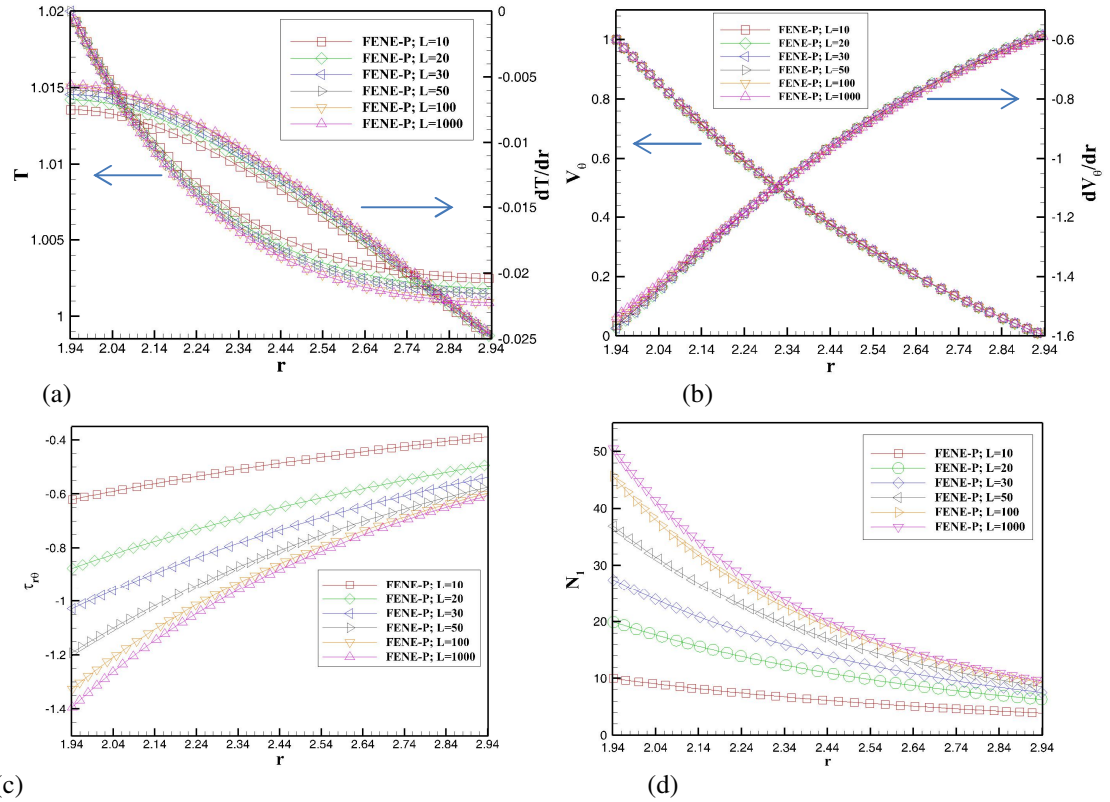


Figure 5 Steady state profiles calculated for *Bi*=10, *Br*=0.0244, *Pe*=20000, β=0.765, ε=0.5 at *De*=13 (a) T^*T_0-273.15℃ (b) V_θ and dV_θ/dr (c) $\tau_{r\theta}$ (d) N_1

The first normal stress is defined as the difference between the normal stress in the flow's direction, $\tau_{\theta\theta}$ and the velocity gradient in direction, τ_{rr}. For the FENE-P model, the first normal stress is presented as

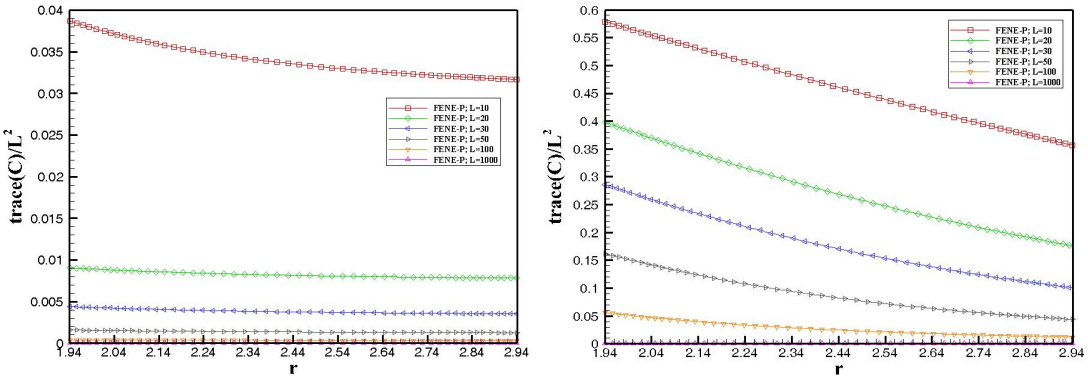
$$\boldsymbol{N_1} = \tau_{\theta\theta} - \tau_{rr} = 2De e^{\varepsilon\lambda\left(\frac{1}{T}-1\right)}\left(\frac{L^2 - [\boldsymbol{C}_{rr} + \boldsymbol{C}_{\theta\theta} + \boldsymbol{C}_{zz}]}{L^2}\right)^2 \left(\frac{-\boldsymbol{v}_\theta}{r} + \frac{\partial \boldsymbol{v}_\theta}{\partial r}\right)^2 \qquad (53)$$

In a similar case using the Oldroyd-B model as the constitutive model, the first normal stress is calculated using the following equation:

$$\boldsymbol{N}_1 = \tau_{\theta\theta} - \tau_{rr} = 2Dee^{\varepsilon_\lambda\left(\frac{1}{T}-1\right)}\left(\frac{-\boldsymbol{v}_\theta}{r} + \frac{\partial \boldsymbol{v}_\theta}{\partial r}\right)^2 \tag{54}$$

Eq. (53) shows that the first normal stress is dependent on the polymer chain extensibility, and this dependency is stated in the multiplying term $\left(\frac{L^2-[\boldsymbol{C}_{rr}+\boldsymbol{C}_{\theta\theta}+\boldsymbol{C}_{zz}]}{L^2}\right)^2$. The multiplying term plays a correction role in Eq. (53) compared to Eq. (54). If $[\boldsymbol{C}_{rr} + \boldsymbol{C}_{\theta\theta} + \boldsymbol{C}_{zz}] = trace(\boldsymbol{C})$ is normalized with L^2, the resulting term expressed mathematically as $\frac{trace(\boldsymbol{C})}{L^2}$, represents as the polymer chain' normalized extensibility.

Fig. 6a and Fig. 6b represent the variation of normalized extensibility across the gap ratio. Regardless of the Deborah numbers, at a fixed point across the gap, the polymer chain's normalized extensibility increases as the polymer chain's maximum extensibility increases. Considering the multiplying factor stated in Eq. (53), it is inferred that the profile of $\frac{trace(C)}{L^2}$ across gap width results in lower values of the normal stresses at a fixed point across the gap.



(a) (b)

Figure 6 Normalized trace(C) across gap for *Bi*=10, *Br*=0.0244, *Pe*=20000, β=0.765, ε=0.5 at a) *De*=0.5 b) *De*=13

4.2. LINEAR STABILITY ANALYSIS: PURELY ELASTIC INSTABILITY VERSUS THERMO-ELASTIC INSTABILITY

Fig. 7 shows the neutral stability curves for the viscoelastic Taylor-Couette flow using similar rheological and geometrical parameters to those of fluid 1. The thermal parameters used are the same used by Al-Mubaiyedh et al. Three of the four eigenfamilies correspond to time-dependent modes of instability. The eigenfamily with $\xi = 1$ is the most dangerous among the three oscillatory modes. In addition to oscillatory modes, there is one stationary ($\sigma_i = 0$) and symmetric ($\xi = 0$) mode for which critical De, is 0.4 and critical axial wavenumber α is about 2.65. This eigenfamily is distinct from all other oscillatory modes. In the calculations used to develop the neutral stability curves represented in Fig. 7, thermal effects are considered; however, if thermal effects are neglected, the most dangerous mode will be the asymmetric ($\xi = 1$) and time-dependent which is in contrast to the non-isothermal case. Fig. 8 represents the neutral stability curve for the most dangerous mode of the instability for isothermal linear stability analysis .

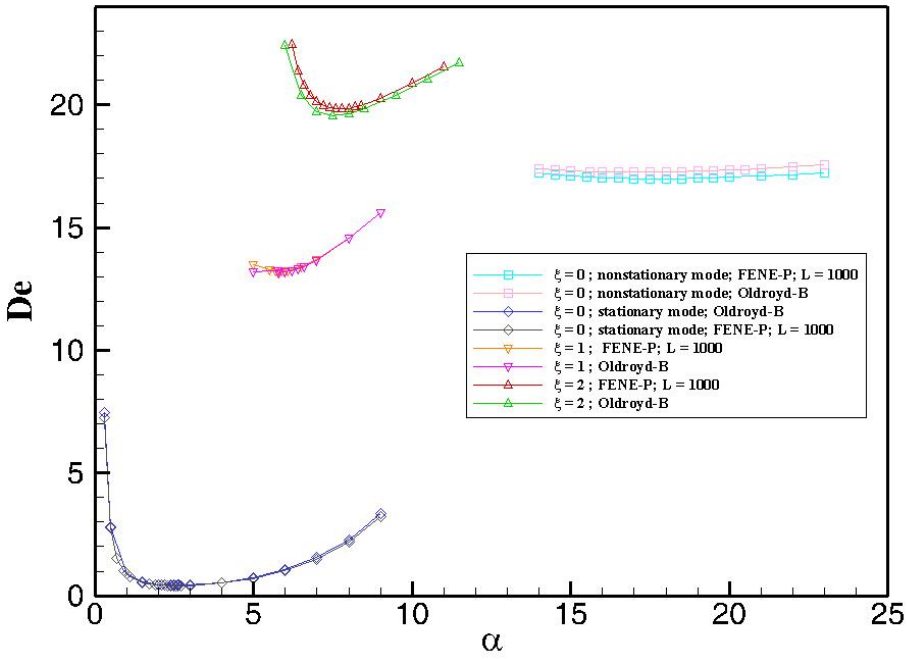


Figure 7 Neutral stability curves for *Bi*=10, *Br*=0.0244, *Pe*=20000, β=0.765, ε=0.5 and *E*=∞

◇ $\xi = 0$, stationary □ $\xi = 0$, oscillatory △$\xi = 1$, oscillatory △ $\xi = 2$, oscillatory

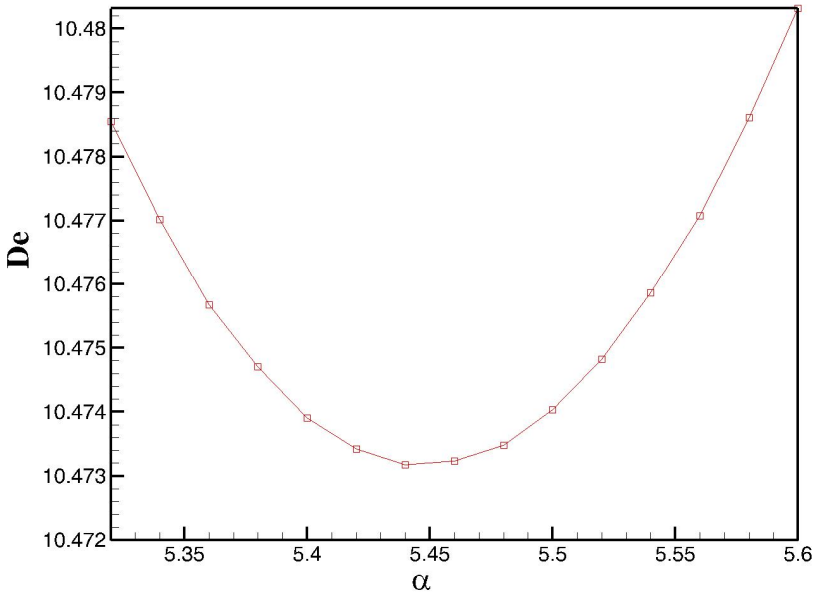


Figure 8 Neutral stability curve for β=0.765 and ε=0.5 using FENE-P model (*L*=1000)

Table 1 summarizes the critical parameters associated with different instability modes for the non-isothermal case and also for the most dangerous mode of instability for the isothermal case.

Table 1 Critical parameters calculated via linear stability analysis (Bi=10, Br=0.0244, Pe=20000, β=0.765, ε=0.5, E=∞)

Isothermal/ Non-isothermal	Azimuthal wavenumber (ζ)	Axial wavenumber (α_c)	De_c
Non-isothermal	0	2.64	0.40
Non-isothermal	0	17.81	16.99
Non-isothermal	1	5.81	13.22
Non-isothermal	2	7.73	19.82
Isothermal	1	5.46	10.47

Boger fluids as suitable model viscoelastic fluids are thermal-sensitive and subjected to a shear field, viscous dissipation occurs which leads to elasticity and viscosity gradients. Comparing the instability modes for both the non-isothermal and isothermal cases, it is deduced that the stationary and symmetric mode can be attributed to the presence of energetic effects leading to a non-uniform temperature distribution.

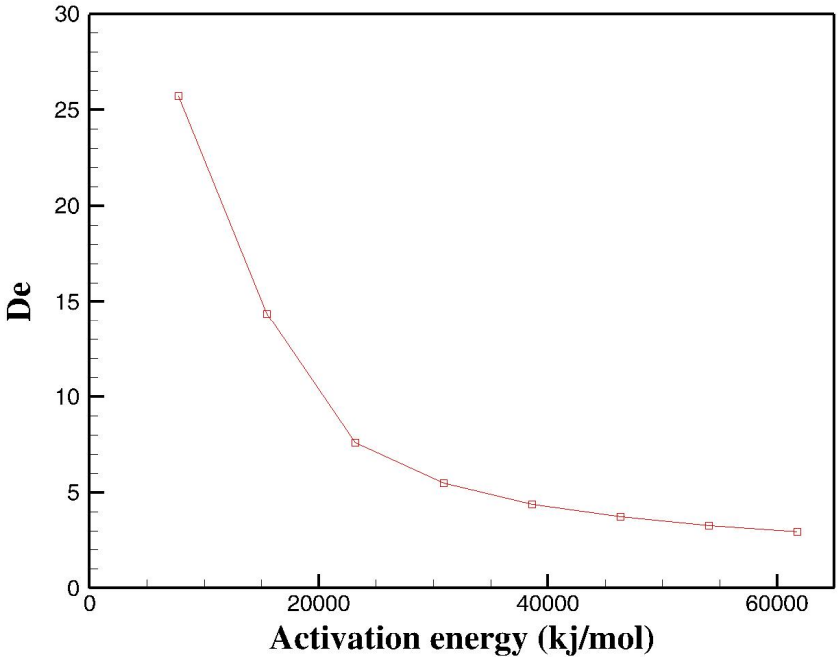
Steinberg et al.'s[17] experiments showed that an abrupt transition occurs in the flow pattern at a De number of approximately 4. They refer to the flow pattern as "elastic

turbulence" with a broad range of temporal and spatial scales. Elastic turbulence appears as a high-order non-linear transition. In the same work, the experiments reveal a critical Deborah number of 1 for the inception of the instabilities which is regarded as the primary flow transition. In the calculations used here, a critical Deborah value of 0.4 is predicted for the system with similar geometrical and rheological characteristics. There is good agreement between the results calculated in current study and the results observed in experiments by Steinberg et al. Moreover, the critical Deborah number for the most dangerous mode of the instability based on isothermal stability analysis is 10.47. This value is an order of magnitude lower than the critical Deborah number of 0.4. Thus, it is concluded that the experiments conducted by Steinberg et al suffer from non-isothermal effects. Hence, the high-order transition flow pattern dubbed "elastic turbulence" should be identified as a "thermal elastic turbulence".

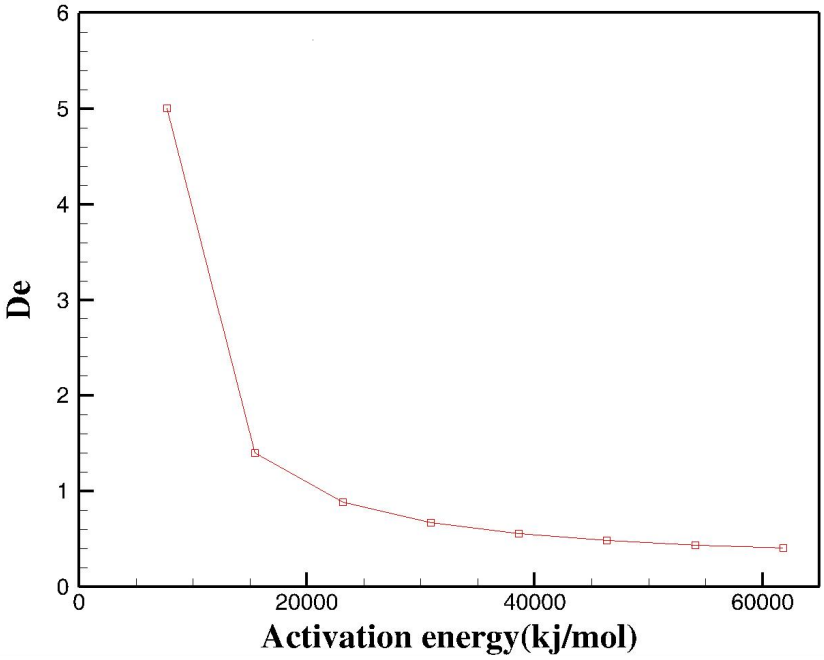
All results reported to this point are based on the activation energy that Quinzani et al. calculated for polyisobutylene solutions.[34] In the next section, the activation energy's effect on instability behavior is investigated.

4.3. INFLUENCE OF ENERGETICS

The activation energy attributed to the viscosity and relaxation time of Boger fluids is about $60{,}000 j/mol$ according to Quinzani et al.[34] However, for more comprehensive insight into the energetic effects, the effect of activation energy on the critical De is investigated. In Fig. 9, such an assessment is presented for a wide gap ratio, $\varepsilon = 0.5$ and narrow gap ratio, $\varepsilon = 0.1$.



(a)



(b)

Figure 9 Critical Deborah (De_c) vs activation energy for Bi=10, Br=0.0244, Pe=20000, β=0.765, E=∞ using FENE-P model (L=1000) (a) ε=0.5 and (b) ε=0.1

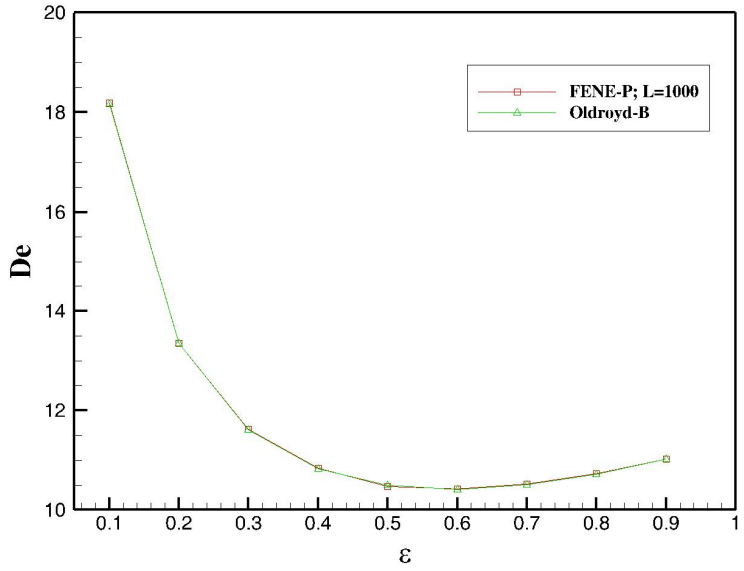
Fluids with a higher activation energy show more thermal sensitivity, leading to even more remarkable viscous dissipation and hence, a lower critical Deborah value for onset of the instability. The results suggest that destabilization caused by thermal sensitivity is not greatly influenced by the gap ratio. This issue is discussed in more detail in the next section.

4.4. INFLUENCE OF GAP RATIO AND SOLVENT VISCOSITY

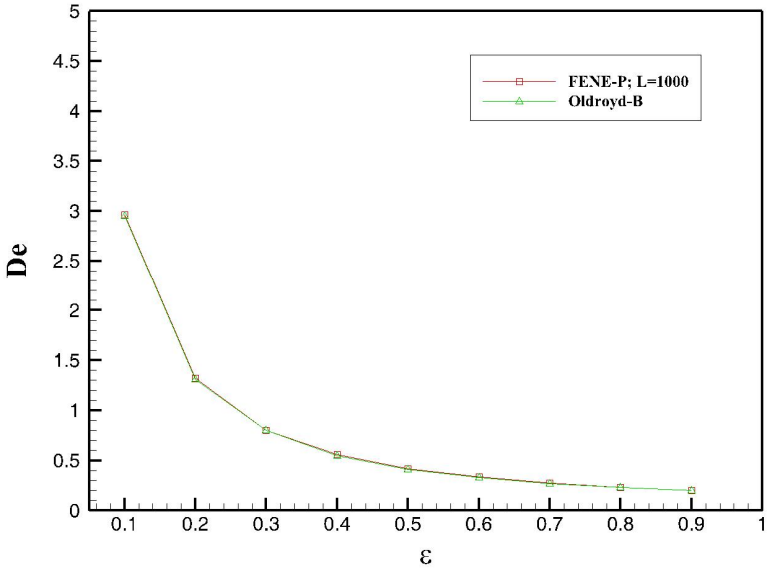
The critical De is evaluated at different gap ratios for both isothermal and non-isothermal cases. In Fig. 10a and 10b, the critical De is depicted versus gap ratio ($\varepsilon = d/R_1$) for the non-axisymmetric ($\xi = 1$) and time-dependent ($\sigma_{Ic} = -0.014492$) mode of the isothermal case ($\beta = 0.765$) and for the symmetric ($\xi = 0$) and stationary ($\sigma_{Ic} = 0.0$) mode of the non-isothermal case ($Bi = 10, Br = 0.0244, Pe = 20000, \beta = 0.765$). Results obtained using the FENE-P model in the limit of $L = 1000$ are compared to those calculated using the Oldroyd-B model in the same figures.

Note that critical De tends to decrease as the gap ratio increases. Polymeric solutions experience normal stresses developed in the direction of the flow and velocity gradient when subjected to a shear flow field. The difference between these normal stresses is known as the first normal stress, which is proportional to the square of the shear rate. When streamlines are curvilinear, these normal stresses form the volume force in the direction of the flow's curvature. This force, called "hoop stress" plays a significant role in developing instability. Thus, as the gap ratio increases due to the higher flow system's curvature, the first normal stresses act even more efficaciously to develop

instability which is followed by intensified hoop causing the onset of instability at lower De values.



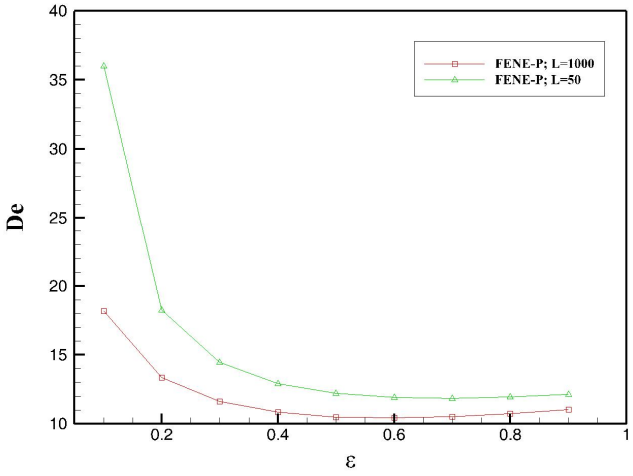
(a)



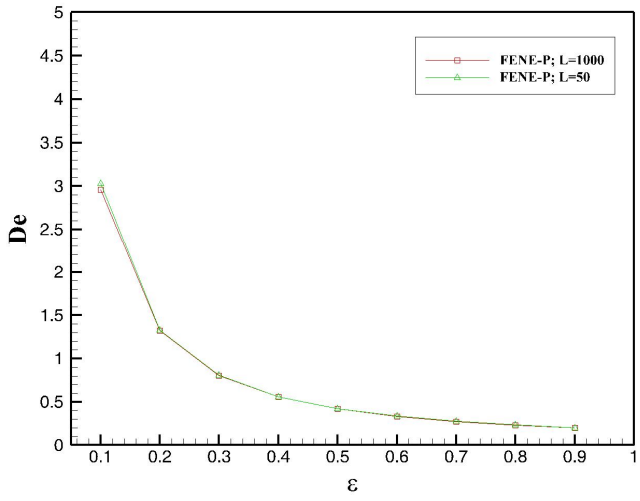
(b)

Figure 10 Critical Deborah (De_c) vs gap ratio for Bi=10, Br=0.0244, Pe=20000, β=0.765 (a) isothermal and non-axisymmetric/time-dependent mode of (ξ=1) and (b) non-isothermal and symmetric/stationary mode of (ξ=0)

The effect of extensibility on the variation of the critical Deborah against gap ratio is depicted in Fig. 11.



(a)



(b)

Figure 11 Critical Deborah (De_c) vs gap ratio for Bi=10, Br=0.0244, Pe=20000, β=0.765 at L=1000 and L=50 (a) isothermal and non-axisymmetric/time-dependent mode of (ξ=1) and (b) non-isothermal and symmetric/stationary mode of (ξ=0)

For lower L ($L = 50$), higher critical De values are achieved for the same gap ratio. As shown in Fig. 11, extensibility leads to a more significant decrease in critical De in the isothermal case as opposed to the non-isothermal case. In other words, the influence of shear-thinning behavior on the time-dependent and non-symmetric modes of instability is more significant than on the stationary and symmetric modes. In Table 2, the critical Deborah at various gap ratios for the most dangerous mode, both isothermal and non-isothermal, with different chain extensibilities is listed.

Table 2 Critical Deborah number calculated via linear stability analysis at various gap ratios for different maximum extensibilities (Bi=10, Br=0.0244, Pe=20000, β=0.765, ε=0.5, E=∞)

Gap ratio(ε)	De_c for L = 50 (Isothermal)	De_c for L = 1000 (Isothermal)	De_c for L = 50 (Non-isothermal)	De_c for L = 1000 (Non-isothermal)
0.1	36.00	18.19	3.03	2.962
0.2	18.24	13.35	1.33	1.32
0.3	14.45	11.62	0.81	0.80
0.4	12.92	10.84	0.56	0.56
0.5	12.20	10.47	0.42	0.42
0.6	11.90	10.42	0.34	0.33
0.7	11.84	10.51	0.27	0.27
0.8	11.96	10.53	0.23	0.23
0.9	12.13	11.02	0.20	0.20

Fig. 12 represents the influence of solvent/solution viscosity ratio on the critical Deborah number. Higher critical Deborah values are achieved as the polymer viscosity's contribution is decreased. The ascending trend in Deborah number is attributed to the reduced effect of normal stresses which play a dominant criterion in developing elastic instabilities.

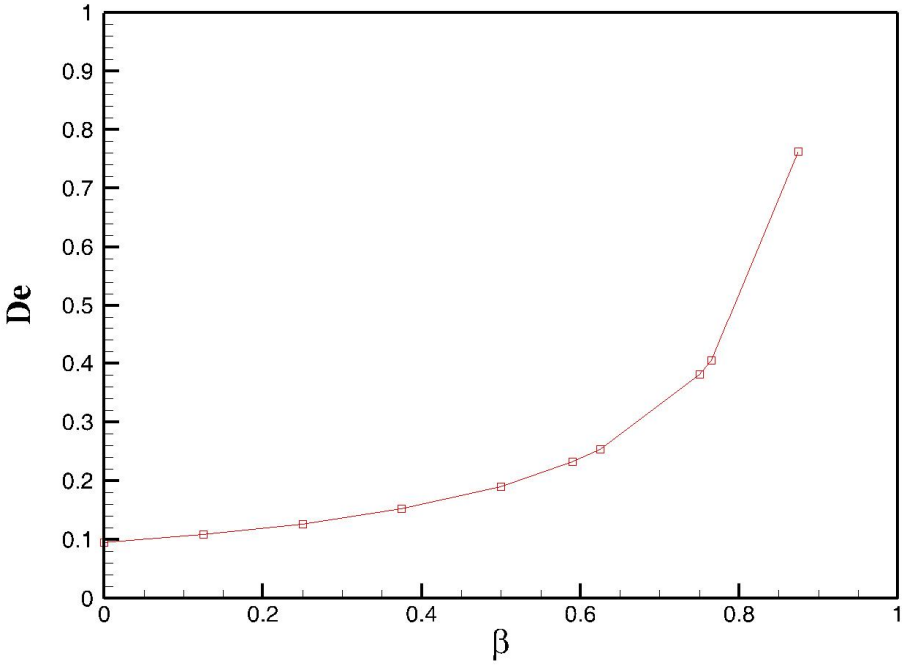
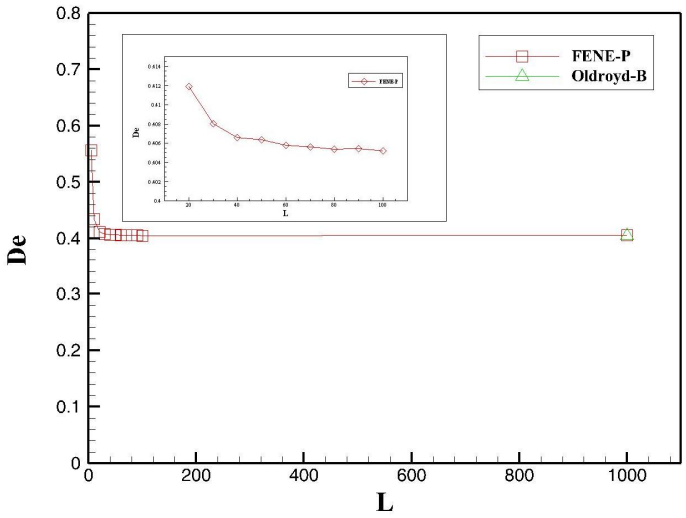


Figure 12 Critical Deborah (De_c) vs solvent to solution viscosity for L=1000, Bi=10, Br=0.0244, Pe=20000, ε=0.5 and symmetric/stationary mode of (ξ=0)

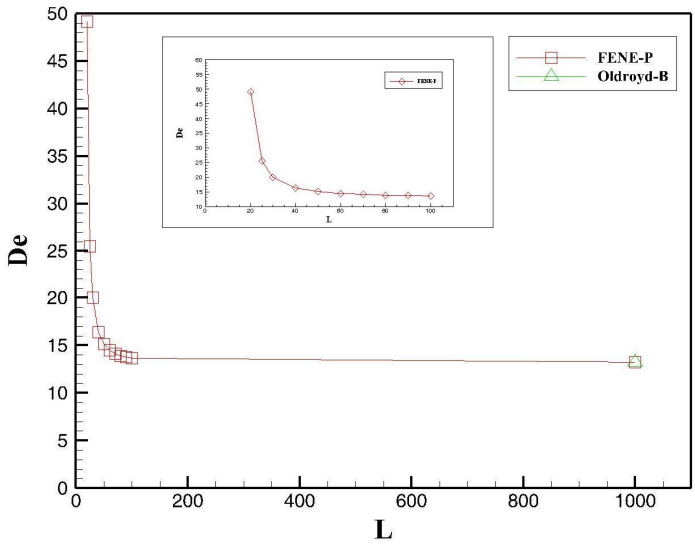
4.5. INFLUENCE OF FINITE EXTENSIBILITY

The effect of maximum extensibility on the critical Deborah number is shown in Fig. 13 for both the isothermal and non-isothermal cases. The critical Deborah decreases as the maximum extensibility is increased. These observations are verified in light of the

dependency of material functions, namely shear viscosity and first normal stress coefficient, on shear rate.



(a)



(b)

Figure 13 Critical Deborah (De_c) vs maximum extensibility (L) for Bi=10, Br=0.0244, Pe=20000, β=0.765 (a) Stationary and symmetric mode (ξ=0) and (b) oscillatory and non-axisymmetric mode (ξ=1)

In Table 3, the critical Deborah number for different extensibilities, both for the isothermal and non-isothermal cases are listed.

Table 3 Critical Deborah number calculated via linear stability analysis at different maximum extensibilities (Bi=10, Br=0.0244, Pe=20000, β=0.765, ε=0.5, E=∞)

Maximum extensibility (L)	De_c for Isothermal Case	De_c for Non-isothermal Case
20	49.145	0.4119
30	25.518	0.4080
40	20.026	0.4065
50	16.403	0.4063
60	15.112	0.4057
70	14.486	0.4056
80	14.130	0.4054
90	13.908	0.4054
100	13.654	0.4053
1000	13.225	0.4051

The FENE-P model predicts shear-thinning behavior in both the shear viscosity and first normal stress coefficient, and Fig. 14 and Fig. 15 represent such shear thinning for both of the material functions. Mathematically, the definition of the shear viscosity based on the FENE-P model in a simple shear flow field is expressed as[23,44]

$$\frac{\eta-\eta_s}{\eta_0-\eta_s}=\left(\frac{L^6}{4\lambda^2\dot{\gamma}^2(L^2-3)^2}\right)^{1/3}\left[(1+A)^{1/3}+(1-A)^{1/3}\right] \tag{54}$$

and the first normal stress coefficient is calculated via the following equation:

$$\frac{\psi_1}{\psi_{1,0}}=\frac{\left(\left(\frac{L^6}{4\lambda^2\dot{\gamma}^2(L^2-3)^2}\right)^{\frac{2}{3}}\left[(1+A)^{\frac{1}{3}}+(1-A)^{\frac{1}{3}}\right]^2\right)}{2} \tag{55}$$

where

$$A=\sqrt{1+\frac{2L^6}{27\lambda^2\dot{\gamma}^2(L^2-3)^2}}$$

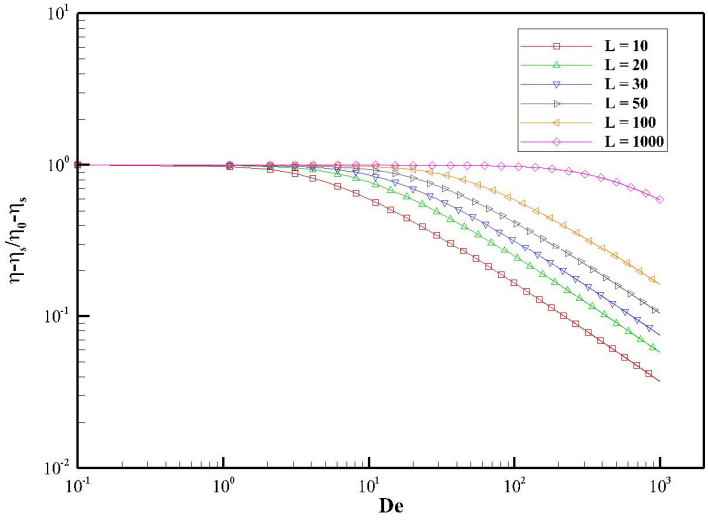


Figure 14 Reduced shear viscosity versus reduced shear rate (defined as *De*) for a dilute solution of FENP dumbbells in a simple shear flow

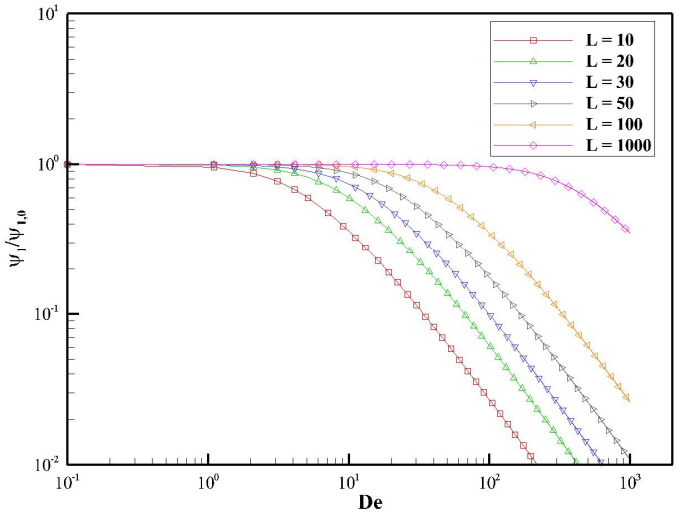


Figure 15 Reduced first normal stress coefficient versus reduced shear rate (defined as *De*) for a dilute solution of FENP dumbbells in a simple shear flow

Fig. 14 represents more significant shear thinning in the shear viscosity for polymer molecules with lower extensibilities leading to lower shear stress. Moreover, the shear stress steady state profile sketched in Figures 4c and 5c reveals that at a fixed radial position, shear stress is decreased as extensibility decreases. Referring to Fig. 15, the shear-thinning behavior of the first normal stress coefficient becomes significant as the *L*'s values decrease. In turn, less normal stress is achieved at lower extensibilities. A similar trend of descending of steady state first normal stress at lower extensibilities is observed in Figures 4d and Fig 5d. At a fixed radial position, higher maximum extensibilities, i.e. higher L values recovers Oldroyd-B model which is incapable of predicting shear-thinning behavior for the material functions; hence, both the shear viscosity and the first normal stress coefficient remain invariant for a broad range of shear rates. Normal stresses play a major role in developing instabilities in viscoelastic

Taylor-Couette flow. Normal stresses will have the highest value at higher extensibilities and subsequently, lower critical Deborah number values are attained at larger extensibilities as shown in Fig. 13. Since polymer chains are considered to be infinitely extensible as predicted by the Oldroyd-B model, leading to the highest possible first normal stress, the lowest possible critical Deborah value is achieved at a stability threshold; this interpretation explains why all other critical Deborah values obtained at finite extensibilities using the FENE-P model are lower than those predicted by the Oldroyd-B model.

CHAPTER 5
CONCLUSIONS

In the current study, the stability behavior of viscoelastic Taylor-Couette flow is investigated by applying two constitutive equations, the Oldroyd-B and the FENE-P models. The primary purpose of this investigation is to examine the hydrodynamic stability characteristics of the flow in presence and absence of thermal effects in the limit of vanishing fluid inertia. Specifically, it has been demonstrated that inclusion of thermal effects lead to significant destabilization of the flow.

The influence of geometrical parameters on the critical Deborah, De_c value has also been investigated. Sweeping through a wide range of gap ratios, a trend of descending critical Deborah number is observed. The effect of the polymer viscosity' contribution on De_c has also been probed. Higher critical Deborah values are achieved at higher solvent to solution viscosity ratios. Finally, the influence of finite extensibility on the De_c has been investigated. Lower chain extensibilities in general give rise to higher De_c. This is attributed to significant shear-thinning of first normal stresses as the chain extensibility is reduced.

LIST OF REFERENCES

1. Taylor, G. I., Stability of a viscous liquid contained between two rotating cylinders. *P R Soc Lond a-Conta* 1923, *102* (718), 541-542.
2. Golubitsky, M.; Stewart, I., Symmetry and Stability in Taylor-Couette Flow. *Siam J Math Anal* 1986, *17* (2), 249-288.
3. Chandrasekhar, S., *Hydrodynamic and hydromagnetic stability*. Clarendon Press: Oxford,, 1961; p 652 p.
4. Chossat, P.; Iooss, G. r., *The Couette-Taylor problem*. Springer-Verlag: New York ; London, 1994; p ix, 233 p.
5. Giesekus, H., Zur Stabilitat Stationarer Und Periodischer Stromungen Viskoelastischer Flussigkeiten in Feldern Mit Geraden Und Gekrummten Stromlinien. *Z Angew Math Mech* 1966, *46*, T198-&.
6. Muller, S. J.; Larson, R. G.; Shaqfeh, E. S. G., A Purely Elastic Transition in Taylor-Couette Flow. *Rheol Acta* 1989, *28* (6), 499-503.
7. Larson, R. G.; Shaqfeh, E. S. G.; Muller, S. J., A Purely Elastic Instability in Taylor-Couette Flow. *J Fluid Mech* 1990, *218*, 573-600.
8. Larson, R. G., Instabilities in Viscoelastic Flows. *Rheol Acta* 1992, *31* (3), 213-263.
9. Shaqfeh, E. S. G.; Muller, S. J.; Larson, R. G., The Effects of Gap Width and Dilute-Solution Properties on the Viscoelastic Taylor Couette Instability. *J Fluid Mech* 1992, *235*, 285-317.
10. Muller, S. J.; Shaqfeh, E. S. G.; Larson, R. G., Experimental Studies of the Onset of Oscillatory Instability in Viscoelastic Taylor-Couette Flow. *J Non-Newton Fluid* 1993, *46* (2-3), 315-330.
11. Shaqfeh, E. S. G., Purely elastic instabilities in viscometric flows. *Annu Rev Fluid Mech* 1996, *28*, 129-185.
12. Steinberg, V.; Groisman, A., Elastic versus inertial instability in Couette-Taylor flow of a polymer solution: review. *Philos Mag B* 1998, *78* (2), 253-263.
13. Thomas, D. G.; Sureshkumar, R.; Khomami, B., Pattern formation in Taylor-Couette flow of dilute polymer solutions: Dynamical simulations and mechanism. *Phys Rev Lett* 2006, *97* (5).
14. Thomas, D. G.; Khomami, B.; Sureshkumar, R., Nonlinear dynamics of viscoelastic Taylor-Couette flow: effect of elasticity on pattern selection, molecular conformation and drag. *J Fluid Mech* 2009, *620*, 353-382.
15. Bird, R. F. C., C. F.; Armstrong, R. C.; Hassager, O., Dynamics of polymeric liquids. 1987, *1 and 2*, Wiley, New York.
16. Pakdel, P.; McKinley, G. H., Elastic Instability and Curved Streamlines. *Phys Rev Lett* 1996, *77* (12), 2459-2462.
17. Groisman, A.; Steinberg, V., Elastic turbulence in curvilinear flows of polymer solutions. *New J Phys* 2004, *6*.
18. Al-Mubaiyedh, U. A.; Sureshkumar, R.; Khomami, B., Influence of energetics on the stability of viscoelastic Taylor-Couette flow. *Phys Fluids* 1999, *11* (11), 3217-3226.
19. Al-Mubaiyedh, U. A.; Sureshkumar, R.; Khomami, B., Linear stability of viscoelastic Taylor-Couette flow: Influence of fluid rheology and energetics. *J Rheol* 2000, *44* (5), 1121-1138.

20. Al-Mubaiyedh, U. A.; Sureshkumar, R.; Khomami, B., Nonlinear stability analysis of viscoelastic Taylor-Couette flow in the presence of viscous heating. *Phys Fluids* 2002, *14* (3), 1056-1064.
21. Crochet, M. J.; Naghdi, P. M., A Class of Simple Solids with Fading Memory. *Int J Eng Sci* 1969, *7* (12), 1173-&.
22. White, J. M.; Muller, S. J., Viscous heating and the stability of Newtonian and viscoelastic Taylor-Couette flows. *Phys Rev Lett* 2000, *84* (22), 5130-5133.
23. Purnode, B.; Crochet, M. J., Polymer solution characterization with the FENE-P model. *J Non-Newton Fluid* 1998, *77* (1-2), 1-20.
24. Baumert, B. M.; Muller, S. J., Flow Visualization of the Elastic Taylor-Couette Instability in Boger Fluids. *Rheol Acta* 1995, *34* (2), 147-159.
25. Baumert, B. M.; Muller, S. J. , Flow regimes in model viscoelastic fluid in a cylinder Couette system with independently rotating cylinders. *Phys Fluids* 1997, *9*, 566-586.
26. Groisman, A.; Steinberg, V., Mechanism of elastic instability in Couette flow of polymer solutions: Experiment. *Phys Fluids* 1998, *10* (10), 2451-2463.
27. Groisman, A.; Steinberg, V., Elastic vs. inertial instability in a polymer solution flow. *Europhys Lett* 1998, *43* (2), 165-170.
28. Avgousti, M.; Beris, A. N., Non-Axisymmetrical Modes in Viscoelastic Taylor-Couette Flow. *J Non-Newton Fluid* 1993, *50* (2-3), 225-251.
29. Avgousti, M.; Beris, A. N., Viscoelastic Taylor-Couette Flow - Bifurcation-Analysis in the Presence of Symmetries. *P Roy Soc Lond a Mat* 1993, *443* (1917), 17-37.
30. Sureshkumar, R.; Beris, A. N.; Avgousti, M., Non-Axisymmetrical Subcritical Bifurcations in Viscoelastic Taylor-Couette Flow. *P Roy Soc Lond a Mat* 1994, *447* (1929), 135-153.
31. Renardy, M.; Renardy, Y.; Sureshkumar, R.; Beris, A. N., Hopf-Hopf and steady-Hopf mode interactions in Taylor-Couette flow of an upper convected Maxwell liquid. *J Non-Newton Fluid* 1996, *63* (1), 1-31.
32. Oztekin, A.; Brown, R. A.; Mckinley, G. H., Quantitative Prediction of the Viscoelastic Instability in Cone-and-Plate Flow of a Boger Fluid Using a Multimode Giesekus Model. *J Non-Newton Fluid* 1994, *54*, 351-377.
33. Al-Mubaiyedh, U. A.; Sureshkumar, R.; Khomami, B., Stability of viscoelastic Taylor-Couette flow: Influence of relaxation spectrum and energetics. *Presented at the 70th Annual Meeting of the Society of Rheology, Monterey, Canada* 1998.
34. Quinzani, L. M.; Mckinley, G. H.; Brown, R. A.; Armstrong, R. C., Modeling the Rheology of Polyisobutylene Solutions. *J Rheol* 1990, *34* (5), 705-748.
35. Arigo, M. T. B., L. E.; McKinley, G. H. , Viscous heating and non-isothermal hydrodynamics in polymer solutions. *Presented at the 70th Annual Meeting of the Society of Rheology, Monterey, Canada* 1998.
36. Al-Mubaiyedh, U. A.; Sureshkumar, R.; Khomami, B., Energetic effects on the stability of viscoelastic Dean flow. *J Non-Newton Fluid* 2000, *95* (2-3), 277-293.
37. Groisman, A.; Steinberg, V., Couette-Taylor flow in a dilute polymer solution. *Phys Rev Lett* 1996, *77* (8), 1480-1483.

38. Groisman, A.; Steinberg, V., Solitary vortex pairs in viscoelastic Couette flow. *Phys Rev Lett* 1997, *78* (8), 1460-1463.
39. Liu, N.; Khomami, B., Polymer-induced drag enhancement in turbulent Taylor-Couette flows: direct numerical simulations and mechanistic insight. *Phys Rev Lett* 2013, *111* (11), 114501.
40. Sureshkumar, R.; Beris, A. N.; Handler, R. A., Direct numerical simulation of the turbulent channel flow of a polymer solution. *Phys Fluids* 1997, *9* (3), 743-755.
41. Leal, L. G., Laminar Flow and Convective Transport Processes. *Butterwoth-Heinemann* 1992.
42. Canuto, C. H., M Y.; Quarteroni, A.; Zang, T. A. , Spectral methods in fluid dynamics. *Springer-Verlag, New York* 1998.
43. John, P. B., Chebyshev and Fourier spectral methods. *Dover Publications, INC., Mineola, New York,* 2001.
44. Wedgewood, L. E.; Ostrov, D. N.; Bird, R. B., A Finitely Extensible Bead-Spring Chain Model for Dilute Polymer-Solutions. *J Non-Newton Fluid* 1991, *40* (1), 119-139.

VITA

Mr. MohammadReza Ghanbari was born in Tabriz, Iran. He studied at Sa'di high school, a high school for talented students. After graduation, he made his way to Tehran, the capital where he obtained a Bachelors in Polymer Engineering from Amirkabir University of Technology (ranked among the outstanding technical universities in Iran) in September 2006. Later, he pursued his academic career at the same university where he accomplished his Masters of Science in Polymer Engineering, Polymer industries in July 2009. He worked as a researcher at Research and Development department of Tabriz Petrochemical Co. for one year. Thereafter, he joined MRAIL (Material Research and Innovative Laboratory) group at the University of Tennessee, Knoxville where he got valuable knowledge on computational simulation of complex fluids. MohammadReza graduated with Masters of Science in Chemical Engineering from University of Tennessee, Knoxville in December 2013. He is continuing his education with a PhD of soft materials at the ETH Zurich, Switzerland.